Progress in plasma-based doping semiconductor photocatalysts for efficient pollutant remediation and hydrogen generation

Tanzim Ur Rahman [a], Hridoy Roy [a], Athkia Fariha [a], Afrina Zaman Shoronika [a], Md. Rashid Al-Mamun [b,c], Syed Z. Islam [c], Md. Shahinoor Islam [a], Hadi M. Marwani [a], Aminul Islam [a], Abdulmohsen K. D. Alsukaibi [a], Mohammed M. Rahman [a], Md. Rabiul Awual [a, d*]

[a] *Western Australian School of Mines, Minerals, Energy and Chemical Engineering, Curtin University, GPO Box U 1987, Perth, WA, 6845, Australia*

[b] *Department of Civil and Environmental Engineering, University of Alberta, Edmonton, Alberta T6G 1H9, Canada*

[c] *Chemical Sciences Division, Oak Ridge National Laboratory, Oak Ridge, Tennessee, USA*

[d] *Materials Science and Research Center, Japan Atomic Energy Agency (JAEA), Hyogo 679–5148, Japan*

*Corresponding author.

E–mail: rabiul.awual@curtin.edu.au (M.R. Awual)

Research highlights:

- Plasma-based doping of composite materials was an efficient way to reduce the band gap.
- Plasma-based doping promoted substitutional doping.
- Different methods for plasma discharge for doping were discussed.
- Limited studies were performed on the real-life applications of plasma-based materials.
- An in-depth understanding of the mechanisms was required for computational modelling.

Graphical Abstract

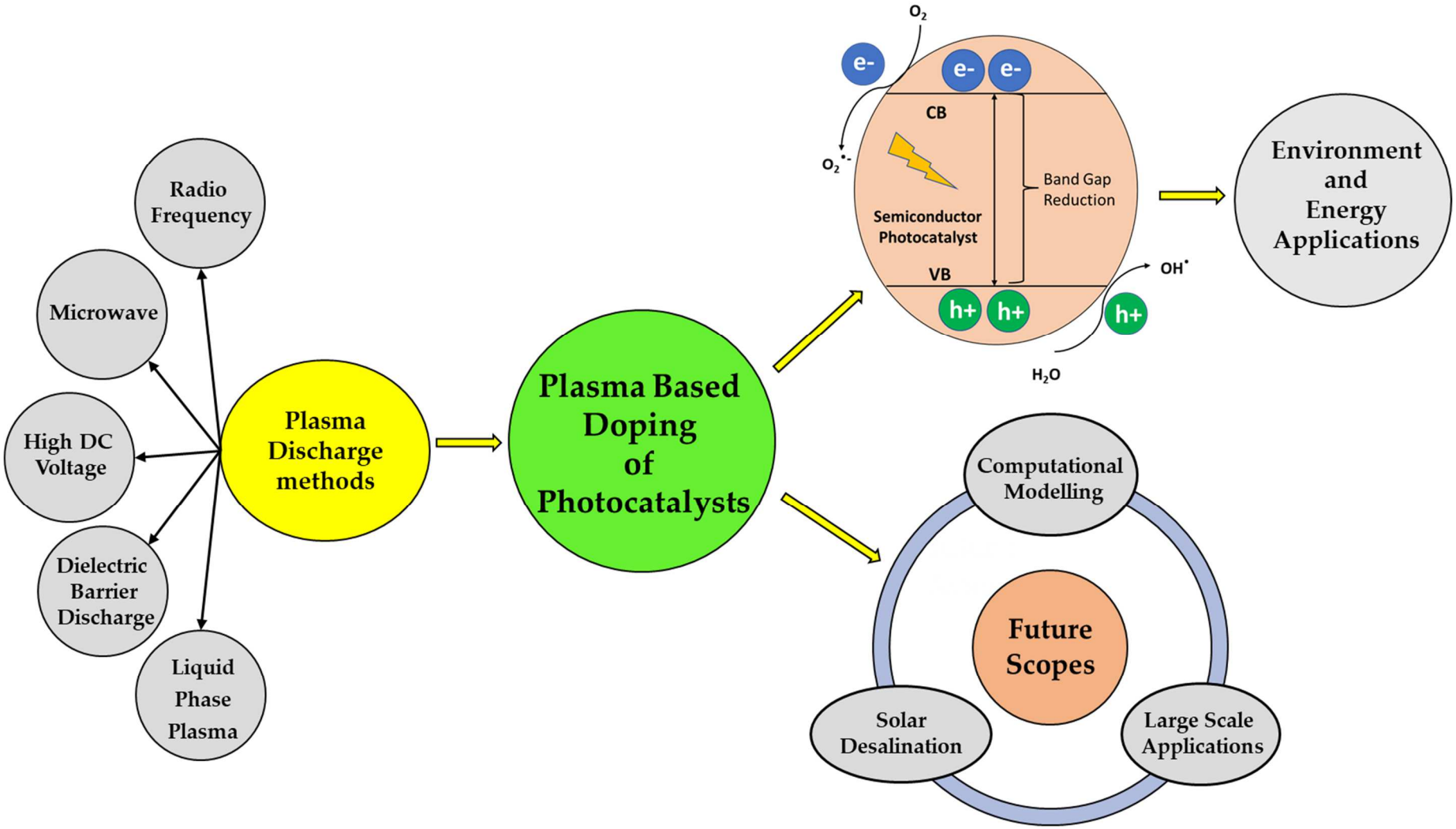

Abstract

In recent years, solar energy-driven photocatalysis materials have drawn significant attention to addressing the global energy and environmental crisis. However, many of the semiconductor photocatalysts are unable to absorb the visible light of the solar spectra due to their wide band gap. The incorporation of a foreign element such as a dopant in the lattice of these photocatalysts was shown to reduce their band gap and enhance visible light absorption. The doping of semiconductors can be performed using several techniques such as sol-gel, hydrothermal, solvothermal, and plasma-based doping. However, plasma-based doping has been considered a highly efficient approach due to the reduction of the band gap to a large extent, enhancement of visible light absorption, and remarkable photocatalytic activities under visible light illumination. The plasma-based doping approach offered many advantages such as high reactivity, process simplicity, scalability, energy efficiency, homogeneous doping, no chemical inventory, low pressure, and low-temperature operation, and flexibility of operation under gas and liquid phase media. Further advancement of plasma-based doping can be achieved through more theoretical studies allowing an in-depth understanding of the mechanisms and interactions of the species involved. This will facilitate the synthesis and application of doped photocatalysts in a cost-effective manner. This review surveyed recent advances in a wide range of semiconductor photocatalysts doped with various dopants using plasma treatment. Various plasma methods for doping semiconductor photocatalysts and their fundamental mechanisms were discussed. The performance characteristics of the plasma-doped photocatalysts were compared to other methods in terms of energy and environmental applications including degradation of environmental contaminants and solar fuel production such as hydrogen production from water splitting using visible light-driven solar energy. Finally, potential future research directions were recommended for the applications of the efficient photocatalysts developed by plasma treatment.

Keywords: Photocatalysis; Plasma doping; Band gap; Environmental remediation; Hydrogen production.

1. Introduction

Currently, the world faces a great challenge in terms of environmental sustainability and energy security [1]. Consumption of fossil fuels for energy production increases environmental pollution through carbon emissions, and their continual depletion poses a huge threat to the global community [2,3]. Furthermore, with industrial progress, hazardous industrial waste disposals are growing, posing a huge concern for the environment [4–8]. As a result, efforts are being made to explore technologies for better utilization of renewable energy sources and environmental remediation [9–11].

Solar energy-driven photocatalysis is a promising approach to solving the existing energy crisis and encountering environmental remediation. Photocatalysis is the process of generation of electron-hole pairs that take part in redox reactions upon the incidence of photons [12]. These redox reactions produce radicals that take part in H_2 production via water splitting, degradation of bio-persistent organic pollutants, CO_2 reduction, disinfection, and other applications [13–15]. Semiconductors are favorable for photocatalysis due to their band gap between the conduction band and valence band being a few electron volts, and band energy alignment with the photocatalytic reactions [16]. The reaction mechanism of photocatalysis involves the generation of electrons and holes upon the illumination of visible and UV light if the incident photon energy is higher than the band gap energy of the photocatalyst. the excited positive charges in the valence band oxidize H_2O to form hydroxyl radical (°OH) while the conduction band electron reduces with pure O_2 to produce superoxide anion radicals ($O_2^{\circ-}$). These strong oxidative species are utilized in the photocatalytic

degradation process and form mineralized products such as carbon dioxide (CO_2), water (H_2O), and other minerals [17–19]. Recently, several semiconductor photocatalysts including TiO_2 [17], WO_3 [18], CdS [20], Bi_3NbO_7 [21], ZnO [22], Cu_2O [23], CdO [24], SnO_2 [25], Al_2O_3 [26], SiO_2 [27], Fe_2O_3 [28], etc. have been employed for different photocatalytic applications because of their enhanced chemical stability, stable electronic structure, and potential chemical and physical properties [29]. Typically, the photocatalytic activity is attributed to increasing visible light harvesting and decreasing the recombination of photogenerated charge carriers [30]. Moreover, due to the formation of the heterostructure, the narrow band gap semiconductors enhance the charge separation and reduce the recombination rate of the photogenerated electron-hole, improving the photocatalytic performance [28, 31–33]. Numerous approaches have been employed to synthesize semiconductor photocatalysts such as sol-gel methods, physical vapor deposition, chemical vapor deposition, chemical precipitation method, spray pyrolysis, microwave-induced plasma technique, solvothermal method, sonochemical method, wet impregnation method, ultrasound impregnation method, hydrothermal method, etc. Each method has specific advantages and disadvantages over the reaction conditions, calcination process, and reactor configuration [34–37]. However, the conventional methods suffer from different disadvantages like high recombination rate, low visible light utilization efficiency, smaller surface area, and pore volume which inhibit their practical application. To address these difficulties, a significant effort has been invested in the development of photocatalysts through suppressing electron-hole pairs, enhancing light absorption capacity, semiconductor coupling, creating point defects, copolymerization, plasma doping, and doping/co-doping of metals/non-metals for improving photocatalytic performance [38]. Doping of photocatalysts can be effective in reducing the band gap causing a redshift of absorption edge for its utilization under solar irradiation. Doping of ions can introduce an additional energy level that can trap the excited

hole or electron reducing the recombination and enhancing charge carrier separation. Also, it can introduce surface defects and oxygen vacancies allowing the reduction of the bandgap. Doping has been found to reduce the band gap allowing photocatalytic activity under visible irradiation, and modification of surface and morphological properties [39]. There are various doping methods including sol-gel [40], chemical vapor deposition (CVD) [41], physical vapor deposition (PVD) [42], hydrothermal [43], and plasma doping [44].

Recently, plasma doping has received greater attention among doping methods from researchers because it is a rapid, facile, and energy-efficient technique. It is widely used in bandgap reduction by inducing defects within the semiconductor photocatalyst allowing enhanced photocatalytic activity [45]. Generally, plasma is a special type of state which consists of a huge number of electrons, photons, free radicals, energetic ions, excited molecules, atoms, and other particles. In the following step, it can be able to initiate a large number of reactions effectively resulting in enhanced surface defects and controlled doping [29,46]. The microwave region (2.45 GHz) has widely been used as the major source which is more readily available. Plasma is formed inside and outside of the bubble's boundary in the liquids whereas bubbles are continuously formed during plasma generation [34]. Furthermore, plasma does not influence the structure of photocatalyst but changes its morphology, introduces active functional groups, improved surface area, and pore volume, increases the hydrophilicity, decreases the bandgap energy, and enhances the separation efficiency of photogenerated electrons/holes and thus consequently increases photocatalytic activity facilitating energy and environmental application [29,47,48]. Studies have shown improved photocatalytic activity by utilizing various types of plasma operating conditions like nitrogen, hydrogen, air, oxygen, and argon. In a recent study, Ramos-Corona et al. (2022) synthesized N-doped ZnO supported on sheets of graphene oxide for the degradation of lignin. They used N_2-plasma discharge for N-doping. They found a reduced band gap

144 resulting in enhanced photocatalytic activity due to plasma doping [49]. In another study,
145 Zhang et al. (2020) demonstrated enhanced transfer and separation of photogenerated charge
146 carriers by applying plasma doping for synthesizing N-doped Cu_2O@CuO heterostructure
147 [45]. The effect of H_2-plasma doping on the photocatalytic activity of TiO_2 was investigated
148 by Yan et al. (2014). The surface defects induced by H-doping resulted in enhanced
149 degradation of MB [50]. It was reported that the plasma doping using O_2-plasma modified the
150 surface morphology, increasing the BET surface area and reducing band gap energy, resulting
151 in enhanced adsorption of rhodamine blue (RhB) dye by g-C3N4 prepared with a
152 hydrothermal technique under anoxic conditions [29]. In another study, Bootluck et al. (2021)
153 demonstrated that the formation of oxygen vacancies and Ti^{3+} was improved by the Ar-
154 plasma treatment of α-Fe_2O_3/TiO_2. This resulted in enhanced photocatalytic performance
155 under visible light illumination [51]. On the other hand, the air plasma treatment of Fe/Co-
156 doped TiO_2 thin films improved their optical absorbance through the formation of Ti^{3+} and
157 oxygen vacancies [52].

158 Although researchers are actively working on several aspects of plasma-doped
159 photocatalysts, a compiled and structured review work in this area is unavailable. Therefore,
160 the production of scattered and non-directional investigative works is dominating in this area.
161 With the goal of solving this issue, in this review, we have summarized the advantages and
162 drawbacks of different doping methods concerning plasma doping. An in-depth discussion on
163 the plasma doping mechanisms was studied to present the holistic idea of plasma doping.
164 Extensive research has been performed on environmental remediation and energy
165 applications using several types of plasma doping. The modeling of the plasma doping area
166 was also investigated based on the literature search. However, a few challenges have been
167 identified by critically reviewing the literature, and the authors have suggested some future
168 recommendations. Finally, the author hopes that this review paper will help find out more

about various types of plasma doping based on their reactor design, reaction conditions, performance, and applications in future research work.

2. Comparative analysis of different doping methods

Several limitations of undoped photocatalysts include insufficient utilization of visible light, high electron-hole recombination, low pollutant degradation, poor thermal stability, and difficulties in the recovery of nanoparticles along with the aggregation of nanoparticles [53]. The photocatalytic properties can be enhanced by doping with metal or non-metal atoms or molecules. Doping enhances photocatalytic activity by narrowing the band-gap energy of the nanoparticles and expanding their activity to the visible region. Various methods employed for doping purposes, e.g., PVD, CVD, sol-gel, hydrothermal, spray pyrolysis, and plasma doping, are represented in **Table 1**. These methods vary in terms of mechanism, cost, chemical, and energy requirement, quality of produced doped photocatalysts, the extent of band gap reduction, etc. Conventional doping methods are effective yet require a substantial amount of chemicals, time, and energy. One of the significant challenges of doping at bulk and nanoscale is that the dopant atoms fail to be incorporated within the nanocrystal lattice and instead get adsorbed on the surface. This is because the defects are thermally unstable and are diffused to the surface of the nanocrystal at the time of growth; in other words, known as self-purification. Another challenge is the inhomogeneous dopant concentration among the nanocrystal [54].

Li et al., (2015) investigated the nitrogen doping of TiO_2 (N-TiO_2) by the sol-gel method [55]. The preparation of N-TiO_2 took 5 days and calcination at 600 °C removed the doped nitrogen. Than *et al.*, (2017) also studied N-TiO_2 by sol-gel method, and the bandgap energy was reduced to 2.71 eV [56]. In both cases, the preparation of the photocatalyst was time-consuming and required the use of many chemicals [55,56]. Sarantopoulos et al., (2009)

194 reported nitrogen-doped TiO_2 by chemical vapor decomposition which resulted in low
195 crystallinity, photo-inactivity, and surface defects at 300-350^{o}C calcination. The bandgap
196 energy was reduced to 3.00-3.05 eV from 3.25 eV [41]. In the case of nitrogen doping for the
197 same semiconductor photocatalyst using plasma doping, Islam et al., 2016 reported that the
198 60-120 min of plasma treatment in nitrogen-doped ordered mesoporous TiO_2 thin film can
199 reduce the bandgap energy 3.5 eV to 2.88 eV. The colorless undoped titania turned into
200 yellow-colored film after plasma treatment and their visible light absorption significantly
201 increased with the redshift of the spectrum (**Fig. 1**). X-ray photoelectron spectroscopy (XPS)
202 suggests that the amount of nitrogen doping in the titania films was about 4.5 atomic % and
203 the doping occurred uniformly across the film thickness. The state of nitrogen in the titania
204 film was substitutional, meaning that the oxygen atom was replaced by the nitrogen atom in
205 the titania lattice. It was suggested that the true band gap is reduced by substitutional doping
206 which was achieved by the plasma treatment. Furthermore, as shown in **Fig. 1**, titania film
207 maintained its nanostructure after the plasma treatment as shown in the scanning electron
208 microscopy (SEM) images (**Fig. 2**). The plasma-treated nitrogen-doped titania films were
209 evaluated by methylene blue degradation using visible light illumination. The doped films
210 degraded methylene blue about 6 times faster than the undoped titania films under visible
211 light illumination. The same group further optimized the plasma processing parameters
212 including power, pressure, and nitrogen gas flow rate into the plasma reactor to obtain the
213 best doping performance. The doped nanostructured titania films were applied to produce
214 hydrogen gas from photoelectrochemical water splitting using visible light of the solar
215 energy. About 200 times higher photocurrent was obtained for plasma-treated titania
216 compared to the undoped titania films under UV-LED, Blue-LED, and Green LED light
217 illumination (**Fig. 3**). The results suggest that plasma treatment in the nanostructured titania

films has a profound impact on its visible light absorption and has shown remarkable performance in photocatalytic performance.

Islam et al., (2016) also reported doping of nitrogen in ordered mesoporous titania films using hydrazine as a chemical precursor for nitrogen [57]. The nanostructured titania films were exposed to hydrazine for about 20 hours. Although nitrogen was doped in nanostructured titania films, XPS showed interstitial doping and a reduced bandgap of 3.3 eV from 3.5 eV. The amount of nitrogen-doped in titania was about 1.0 - 2.0 atomic%. The results suggest that compared to the chemical method, plasma-based doping showed significantly higher photocatalytic performance. The results suggest that plasma-based doping is much more efficient than wet chemical-based doping in nanostructured titania photocatalysts. As shown in **Table 1**, the plasma doping method for the same N-TiO_2 catalyst requires less time and chemicals compared to the aforementioned methods [44,58, 116-121, 124-127].

In addition to improving photoactivity, plasma doping has great economic potential for large-scale applications compared to other methods. The cost of plasma doping mainly involves fixed and operational costs. The fixed expenses mainly include the cost of the plasma reactor and overall setup. On the other hand, the operating costs include the cost of energy and dopants used in the discharge [59–61]. The enhanced photoactivity of the plasma-doped photocatalysts should be taken into account while assessing the economic potential of the process. Compared to other techniques, the plasma doping method is cost-effective as it does not require any catalysts, surfactants, and other chemicals. It only requires dopant precursors. Furthermore, plasma doping using nonthermal plasma is a fast, flexible energy-efficient, and sustainable process [61,62]. The plasma reactor can be optimized by tuning the operating parameters for achieving controlled doping. With further modifications, higher yield and reduction of cost can be achieved by scaling up the plasma reactor [46]. In spite of

having great economic potential compared to other processes, there has been no study conducting the economic analysis of plasma-doped photocatalysis. As a result, there is a scope for investigation regarding the economics of the plasma-doping method in order to assess its application on a large scale.

Plasma doping is not only effective but also overcomes the difficulties associated with the other methods. Doping using plasma produces a more homogeneous distribution of doped materials and energy. It also reduces doping time owing to the single-step treatment and causes less consumption of chemicals, thus decreasing cost. However, all types of plasma doping methods do not provide the same benefits. For instance, the nanostructure of many photocatalysts may not be completely stable under thermal plasma conditions. Non-thermal plasma is easier to handle, relatively safer, environmentally friendly, and cheaper compared to thermal plasma [63]. It also maintains the nanostructure of the photocatalyst due to low-temperature treatment [58]. Regardless of the differences between various plasma doping methods, plasma generally produces more uniform doping, higher degradation and reaction rate, and higher substitutional dopant on the surface of the nanocrystal [64,65]. Therefore, plasma doping can be considered a better approach compared to other conventional methods.

3. Plasma-Based Doping of Semiconductor Photocatalysts

Plasma is known as the fourth state of matter containing excited electrons, ions, radicals, and photons. It is formed when the atoms of the dopant obtain sufficient energy such that the electrons are released from the atoms. As a result, positive nuclei and free electrons are formed in the gaseous state. This ionized state is electronically neutral due to the presence of an equal number of electrons and positively charged nuclei. The plasma thus formed is highly reactive compared to the gaseous state of the dopant which enhances the doping

efficiency of the atoms in the photocatalyst [9]. In addition to thin films, photocatalyst powder or nanotube arrays can also be plasma-doped [58]. If enough energy is available, plasma doping can also be carried out in both liquid and gaseous phases. It is mainly done in a vacuum or low pressure.

3.1. Mechanism of Plasma Doping

For the deposition of dopants or doping by plasma, the fast-moving electrons collide with the particles. These collisions can be elastic or inelastic. When an inelastic collision occurs, it causes a change in the potential of the particles. As a result, excitation, ionization, and dissociation of the particles occur, as shown in **Fig. 4.**

In this situation, the plasma reaches a quasi-neutral condition. The region between the plasma and the substrate or thin film is known as the sheath region. In the positively charged sheath region, the neutral species migrate by diffusion and the ionized particles accelerate through the sheath layer to reach the thin film where it is bombarded to cause reaction, adsorption, and dissociation. For doping, these high-energy particles take the interstitial spaces and cause surface defects on the photocatalyst to which they are to be doped. The by-products formed are desorbed from the surface [66]. In the case of plasma doping with nitrogen, precursors such as NH_3, and N_2 are used. An inert gas such as Ar is also utilized with the precursors for the creation of oxygen vacancy allowing substitutional doping of nitrogen atoms [51]. Furthermore, it can take part in the penning ionization process by the metastable Ar atoms [67]. Moreover, argon helps in igniting the plasma before introducing the dopant species such as nitrogen. Using NH_3 as a precursor, Chen et al., (2019) synthesized N-doped TiO_2 using cold Dielectric Barrier Discharge (DBD) plasma. It was found that both substitutional and interstitial doping of N occurred because of DBD plasma which is evident from the XPS results as shown in **Fig. 5** [67].

The optical emission spectra showed the formation of reactive species in the plasma including NH and N_2^+ radicals. The concentration of N in TiO_2 is found to increase as the concentration of NH_3 and power increase. Since the amount of N in TiO_2 is dependent on the NH radical formation, the NH formation is reduced at a high concentration of NH_3 due to its decomposition to H^- and NH^- [58], [59]. They proposed that the reactions take place allowing the formation of NH radicals as shown below [67–70]:

Ionization and Excitation Reactions:

$e^- + NH_3 \rightarrow NH_3^* + e^-$	(1)
$e^- + NH_3 \rightarrow NH + 2H + e^-$	(2)
$NH_3^* + e^- \rightarrow NH + 2H + e^-$	(3)
$e^- + NH_3 \rightarrow NH_3^+ + 2e^-$	(4)
$e^- + NH_3^* \rightarrow NH_3^+ + 2e^-$	(5)

Penning Reaction with Argon:

$Ar + NH_3 \rightarrow NH_3^+ + Ar + e^-$	(6)
$Ar + NH_3 \rightarrow NH_2 + Ar + H$	(7)
$Ar + NH_3 \rightarrow NH + Ar + H + H$	(8)

Binary and Three-body reaction:

$NH_2 + Ar + H \rightarrow Ar + NH_3$	(9)
$NH_2 + NH_2 + Ar \rightarrow Ar + N_2H_4$	(10)
$go + H + H + Ar \rightarrow Ar + NH_3$	(11)
$H + H + Ar \rightarrow Ar + H_2$	(12)
$NH + NH \rightarrow 2H + N_2$	(13)
$NH_2 + N \rightarrow 2H + N_2$	(14)

303 Studies have also shown the plasma doping of N into the lattice of TiO_2 using an N_2
304 precursor. The reactions for N_2 plasma are simple with the formation of the excited state of
305 nitrogen and radicals and are as follows:

Excitation Reaction: $N_2 + e^- \rightarrow N_2^* + e^-$	(15)
Radical Formation: $N_2^* + e^- \rightarrow N + N + e^-$	(16)

306

307 Islam et al., (2016) observed that N_2/Ar plasma-treated TiO_2 contained a larger
308 amount of substitutional N bond in the lattice from XPS results [58]. This can be attributed to
309 the application of Ar and plasma doping, which causes oxygen vacancies in the lattice and
310 allows the production of a more intense substitutional XPS peak compared to other doping
311 techniques, hence enhancing the photocatalytic activity compared to other techniques.

312

313 **3.2 Properties of plasma doped photocatalysts**

314 Plasma-doped photocatalyst shows enhanced photocatalytic activity. The
315 enhancement of photoactivity is mainly achieved by the reduction of the band gap. Plasma
316 treatment of photocatalysts allows the increase of oxygen vacancies and introduces defects
317 within the structure of the catalyst [52,71].

318 Oxygen vacancies generated in metal oxides through plasma doping can play a
319 significant role in enhancing photoactivity. It has an enormous impact on the photocatalytic
320 redox reactions. It can control light absorption and charge separation by forming defective
321 sites and lattice distortion [72,73]. It can create new defect levels allowing a downward shift
322 of the conduction band and an upward shift of the valence band. As a result, the band gap is
323 narrowed which allows enhanced photocatalytic activity under solar irradiation. Oxygen

vacancies can also control the transfer of charges and recombination rate. It can trap electrons by acting as positive charge centers inhibiting the recombination of electron-hole pairs [74]. However, excessive oxygen vacancies can trap more electrons and inhibit their movement. As a result, the excessive formation of oxygen vacancies can lead to a reduction in photocatalytic performance [75]. Plasma doping can prevent excess oxygen vacancy formation as it is controllable and allow proper distribution of defects throughout the catalyst surface [46]. Other than that, oxygen vacancies can enhance the adsorption of molecules and control the kinetics of photocatalytic reactions. Oxygen vacancies formed due to plasma allow substitution doping. Several characterization techniques including XPS, Raman spectroscopy, Electron Paramagnetic Resonance (EPR), Scanning Transmission Electron Microscopy (STEM), etc. and can be used to investigate oxygen vacancies [72]. The substitutional doping can increase the photoactivity of the nanocomposites as shown in the previous section. Plasma doping has also been shown to increase the surface area and modifier of surface morphology of the catalyst resulting in more active sites for photocatalytic reaction.

4. Plasma Discharge Methods

Various types of plasma can be used for doping photocatalysts. The plasma doping methods include (i) plasma enhanced chemical vapor deposition (PECVD), (ii) liquid phase plasma (LPP), (iii) arc discharge, (iv) ion implantation, (v) corona discharge, (vi) microwave plasma discharge (MPD), (vii) radio frequency plasma discharge (RFPD), and (viii) DBD. Each of the mentioned methods has both advantages and disadvantages that keep their significance distinct from each other. It is possible that sometimes one method can be suited better for a certain photocatalyst whereas others cannot be used effectively. For example, because of high energy consumption, and low yield, the arc discharge method cannot be used

industrially whereas, CVD can overcome those shortcomings [76]. All the methods have different applications based on their modification properties. The arc discharge is used for fuel conversion, whereas corona discharge is used not only for fuel conversion but also for combustion. PECVD is mostly used for passivation, DBD for the main basic research study, and, MPD and RFPD for syngas production.

4.1 Radio Frequency based plasma

In the case of radio-frequency (RF)-based plasma, the plasma is generated using a radio frequency of 13.65 MHz [76,77]. It uses two electrodes including RF biased electrode and a ground electrode. The RF-biased electrode is connected to the RF power source through an impedance-matching network [78]. The plasma remains in the space between the two electrodes. Depending on the coupling of the power source to the plasma, there can be two types of discharge namely, Capacitively Coupled Plasma (CCP) and Inductively Coupled Plasma (ICP). In plasma doping applications, ICP is used more compared to CCP. The ICP is more suitable for semiconductors and metal etching compared to CCP [79]. **Fig. 6** shows the schematic of the plasma reactor using RF power with a matching network and using ICP discharge.

Literature has also shown the use of RF assisted by magnetron sputtering for plasma doping [80]. Magnetron sputtering increases the rate of ionization followed by plasma density by the introduction of a magnetic field [81]. It is common for the preparation of thin films. Liu, Wen, and Zhao, (2008) synthesized a thin film of N-doped TiO_2 using the radio frequency magnetron sputtering technique, which showed an increase in the composition of N as well as photocatalytic activity as the power of sputtering increased [80].

4.2 Microwave-based plasma

For doping photocatalysts, the MPCVD system is commonly used for the generation of plasma of dopant atoms. In the MPCVD reactor, the microwaves of 2.4 GHz generate an electric field which causes the formation of the plasma of the dopant molecules [82]. The microwaves interact with the free electrons remaining in the gas produced by radiation and thermal energy to cause oscillation. These oscillating electrons interact with other atoms and molecules to induce a higher degree of ionization [83,84]. This plasma of the dopant molecules deposits on the photocatalyst to be doped at low pressure. **Fig. 7** shows the plasma reactor using Microwaves for the plasma generation and deposition of dopants in the host photocatalyst.

The MPCVD reactor does not require any internal electrodes diminishing the risk of electrode contamination. This allows the production of a thin film of high purity. This process operates at a higher frequency which causes the generation of high-density plasma compared to the RF plasma process. Furthermore, microwave-assisted plasma is preferred due to its greater controllability [80]. Islam et al., (2016) synthesized a mesoporous thin film of TiO_2 which was doped using N_2/Ar plasma treatment to evaluate its photocatalytic activity [58]. It was found that the plasma treatment by MPCVD resulted in efficient doping of N atoms by the higher energy of the plasma and disorderliness within the molecules which enhanced the photocurrent compared to the undoped films.

4.3 High DC voltage-based plasma

Another way of plasma doping can be performed is by using a high-voltage DC source. Plasma is generated by applying a negative voltage to the cathode which causes the formation of a large electric field in the sheath region. The electrodes also require a cooling system to prevent them from overheating. Subsequently, the photocatalyst is doped using the plasma of dopants [76,85]. Although a high deposition rate can be achieved through this

process, it has some limitations [86]. The limitation is its use for the deposition of insulating materials. It causes an accumulation of charge on the insulating material which has a diminishing effect on the plasma. A large portion of the input power is also used to accelerate the ion and generate plasma. Thus, the high voltage applied can cause damage to the thin films or the substrates [66,76]. Despite its limitations, this process for plasma generation is utilized for both liquid and gas-phase plasma because of its simple installation and operation. Gholami et al., (2021) used a plasma reactor shown in **Fig. 8** operated by a high voltage (1200V) DC source for doping of N in WO_3 incorporated mesoporous carbon photocatalyst which caused the reduction of bandgap and enhancement of photocatalytic activity [87].

4.4 Dielectric barrier discharge (DBD) plasma

DBD plasma is often used for plasma doping. It is a type of non-thermal plasma generated by applying high AC voltage between electrodes which are isolated by dielectric materials such as quartz, polymer, silica, etc. [88]. The dielectric barrier helps in limiting the discharge current and distributing the plasma in the space between the electrodes. DBD plasma can operate at low temperatures and under atmospheric pressure without requiring a vacuum which makes the process simple and low-cost [89]. In the case of plasma doping, DBD plasma generates electrons with high energy which interact with the precursor or dopant gas to form radicals and excited species which occupy the places within the lattice of photocatalyst as interstitial or substitutional atoms. Plasma doping can be carried out in mainly two ways. One of the ways is where the discharge gas and dopant precursor are different. Another way is where the discharge gas is used as the dopant precursor [67,89].

Zhu *et al.*, (2019) used ammonium bicarbonate and boric acid for doping nitrogen and boron in Graphene Oxide (GO). The DBD plasma treatment was performed using H_2 as

discharge gas which caused the formation of nitrogen and boron radicals. These radicals introduced structural defects in GO. This doping resulted in enhanced electrical capacitance of the doped GO composites.

Chen *et al.*, (2019) doped Nitrogen within the lattice of TiO_2 using DBD cold plasma where the discharge gas was NH_3/Ar. In this case, the discharge gas is used as the dopant precursor. **Fig. 9** shows the experimental setup for N-doping. **Fig. 9(a)** shows the DBD reactor system which contains two copper electrodes between which the plasma is generated. Here, the alumina barrier of 3 mm was used between the electrodes. The high-voltage electrodes are connected to an AC power supply. The doping caused the enhancement of photocatalytic activity with a reduction of the band gap. The substrate is placed on the bottom electrode. On the other hand, **Fig. 9(b**) depicts the plasma doping process where an annealed thin film of TiO_2 is doped using the NH_3/Ar plasma. The flow of NH_3 and Ar are controlled and supplied from their respective cylinder. Before plasma generation, the system is purged with NH_3-removed air to create an inert atmosphere. The flow rates are controlled to vary the concentration of N-doping of TiO_2. Other studies that used DBD plasma treatment include H_2/CCl4-treated TiO_2 [91], Sulphur doped carbon nitride [92], and O_2-doped MoS_2 [93]. All the photocatalysts doped by DBD plasma have shown enhanced photocatalytic activity.

4.5 Liquid Phase Plasma (LPP) Process

In recent years, LPP is widely used for doping nanomaterials which enhances their photocatalytic activity [94]. The advantage of plasma doping using LPP is that it does not require any reducing agent. The doping is performed by the formation of highly active species within the liquid [95–97]. The plasma can be generated in the liquid medium in two ways [98]. The first method is the streamer discharge where plasma is discharged in small channels, as shown in **Fig. 10(b)**. In this streamer discharge method, the density of liquid

near the electrode is reduced, causing the formation of cavitation bubbles by the high overvoltage electric field or the collision of electrons with the liquid [99]. Another LPP method is the plasma in bubbles. In this method, the plasma is formed inside the bubbles as shown in **Fig. 10(a).** Under high voltage, bubbles are formed by the evaporation of water caused by joule heating. When a required threshold voltage is applied, plasma is formed within the bubbles which coalesce under the electric field to create a continuous channel of plasma between the electrodes [100]. The analysis of the plasma produced in liquid shows the formation of OH radicals, atomic H, and atomic O. This proves the plasma is formed due to the excitation of water molecules in the bubble rather than air. Sometimes the analysis shows the presence of atomic N due to the dissolution of air [98,99,101]. The drawback of LPP is the melting of the electrodes and contamination of the products as the electrodes are immersed within the solution. To address this challenge, the choice of electrode material is significant. For ultrasonic homogenizer coupled with the microwave antenna electrode can be used for the efficient generation of plasma within the bubbles and to reduce the surface deterioration of the electrode materials [99,102].

The plasma can be generated depending on the electrode arrangement using AC power, high DC voltage, Microwave or RF, and laser ablation technique. Jung et al., (2022) used the LPP process using a high-voltage power supply to generate plasma, and pulsed plasma discharge was used to prevent the deterioration of the electrodes [103]. The $Eu(NO_3)_3.5H_2O$ precursor solution was used for plasma doping of Europium oxide on TiO_2 which showed enhanced photocatalytic activity. Sang-Chul Jung and his coworkers reported enhanced photocatalytic activity by plasma doping using LPP using the setup mentioned above. They have synthesized WO_3-doped TiO_2 [104], Fe-N-doped TiO_2 [94], Iron oxide-doped TiO_2 [105], and Eu and N co-doped TiO_2 [106]. These doped photocatalysts showed enhanced photocatalytic activity. The enhanced photocatalytic activity was evident as there

was a reduction of band gap by values up to 0.25 eV. Also, it was evident through the enhanced degradation of pollutants. The enhanced photocatalytic activity was evident by the reduction of band gap up to 0.25 eV and it was evident through enhanced degradation of pollutants such as Acid Orange, Methylene Blue, Diethyl Phthalate, and Diclofenac. **Table 2** depicts each type of plasma with its benefits, limitations, and scopes of application [9, 66, 98, 99, 128-131].

5. Plasma-doped photocatalyst

In recent times, nano photocatalysts are being used for various purposes in different environments. The photocatalytic activity and usability can be significantly improved by the doping process, as doping provides improved surface properties, reduction of bandgap energy, and restricts the recombination of electron-hole pairs. Previously the advantages of plasma doping over other methods have been thoroughly discussed. In plasma doping, metals, non-metals molecules, and atoms, different types of gases are incorporated with varieties of nano-catalysts using different methodologies. Several researchers reported different plasma treatment methodologies on the photo-catalyst to obtain smaller particle size, wider light absorption range, reduced bandgap energy, and improved charge separation efficiency with enhanced photocatalytic activity. The plasma has been applied to treat a wide range of photocatalysts with various dopants. The photocatalysts include TiO_2, Cu_2O/CuO, CdS, and ZnO. The dopants include non-metals e.g., nitrogen, and hydrogen, and metals e.g., iron (Fe), silver (Ag), copper (Cu), and europium (Eu). The doped photocatalysts have been used for diverse applications including dyes and organic pollutants degradation, and photoelectrochemical water splitting-based hydrogen production under visible light of solar energy.

Plasma-doped photocatalysts have been utilized to degrade organic dye from an aqueous solution. In plasma-treated photocatalysts, nitrogen distribution is more uniform throughout the depth of the film than in the conventional doped catalyst, which increases the catalytic characteristics and degradation performances. Hyun Uk Lee et al. (2014) reported the photocatalytic characteristics of plasma-treated nitrogen-doped nanoporous TiO_2 (N-TiO_2) for the degradation of Rhodamine B dye [107]. The radio frequency generator used argon (Ar) as carrier gas and N_2 as reactive gas to synthesize the N-TiO_2. The synthesized N-TiO_2 showed increased surface area (375.9 m^2 g^{-1}) compared to commercial anatase TiO_2. The band gap was reduced and high photostability was obtained with N-TiO_2. Moreover, N-TiO_2 exhibited an accelerated transformation from anatase to rutile phase at low annealing temperature with increased photocurrent density. Islam et. al. (2016) reported the N-doped mesoporous TiO_2 thin film synthesis and its photocatalytic activity [58]. The sample was purged with Ar at 100 standard cubic centimeters per minute (sccm) in the MPCVD system at an N_2 flow rate of 40 sccm. The synthesized N-doped TiO_2 showed uniform N_2 distribution through the depth of the film and a reduced bandgap energy of 2.88 eV. The dye degradation rate coefficient and photocurrents increased by 6 times and 80-240 times, respectively. Wenxia Zhao et al. (2019) reported the preparation and photocatalytic activity of plasma-treated N-TiO_2 for the degradation of methyl orange dye [65]. The non-thermal plasma (cold plasma) process was followed to avoid surface reduction and defects due to the sintering of the photocatalyst. The conventional N-TiO_2 prepared by the sol-gel method was treated in a DBD reactor for 30 min at 15 W with an N_2 flow rate of 450 mL/min. The plasma-treated N-TiO_2 showed a reduced bandgap energy of 1.7 eV compared to the conventional N-TiO_2 (~3.0 eV). The reaction rate was ~2.8 times higher and about 35 % greater MO degradation was achieved in plasma-treated N-TiO_2. P. Manojkumar et. al. (2020) utilized plasma electrolytic oxidation (PEO) on transitional metal-doped (Mo/V/W) TiO_2 for the mineralization of MB

dye [108]. In an immobilized photocatalytic surface, doping materials (Mo/V/W) were added to commercial pure TiO_2 and treated with PEO for 8 min with 150 mA/cm^2 current density, which subsequently restricted the formation of rutile phase in TiO_2 and increases the surface area. Higher charge separation efficiency, low recombination rate, and increased mineralization of MB dye were obtained with plasma-doped TiO_2. Moreover, plasma-treated photocatalysts have been reported to be successfully used in different areas. Cheng-Yen Tsai et al. (2013) reported the gaseous low-concentration mercury (Hg) removal by Cu-doped TiO_2 treated with atmospheric pressure thermal Ar/O_2 plasma with a DC non-transferred plasma torch [109]. Peimei Dong et. al. (2019) reported the green synthesis of N-TiO_2 nano-photocatalyst by H_2 cold plasma treated Ag deposition [64]. The sample was placed in a DBD reactor where Ar-H_2 is pumped at 50 L/min for 5min. Recently, some researchers have reported the utilization of the liquid phase plasma process (LPP). Seo Jin Ki et. al. (2019) reported the facile synthesis of tungsten oxide doped TiO_2 photocatalyst by LPP and utilized it to degrade diethyl phthalate [104]. The LPP-treated TiO_2 exhibited specific surface area reduction (by blocking mesopores) and enlarged pore diameter, which improved the photocatalytic activity. The synthesized photocatalyst `gave 1.7 to 6.2 times more degradation of under blue light diethyl phthalate compared to TiO_2. In another study, Sang-Chul Jung et. al. (2022) assessed the photocatalytic activity of LPP-treated europium (Eu) doped TiO_2 (Eu-TiO_2) for the mineralization of acetylsalicylic acid [106]. For the preparation of the photocatalyst, powder TiO_2, and Eu precursor was dispersed in a cylindrical quart batch reactor and direct pulse type plasma was used to prevent corrosion of electrodes. In the LPP-treated photocatalyst, Eu was uniformly precipitated on the TiO_2 surface from the precursor and atomic oxygen % increased significantly, which showed enhanced photocatalytic activity to degrade acetylsalicylic acid. Semiconductors other than TiO_2 have also been used doped using plasma-based methods for different applications. In another

study, Lixiang Zhang et. al. (2021) used plasma-assisted nitrogen doping to form CdS/N-CoSx (cadmium sulfide/N-doped cobalt sulfide) for photocatalytic Cr (VI) reduction. The plasma doping introduced enhanced surface wettability and conductivity. The facilitated Co-N bonds showed the best photocatalytic activity for 5 min of plasma treatment [110]. **Table 3** summarizes different plasma-doped photocatalysts and their environmental applications [58, 64, 65, 103, 107-110, 132, 133].

The plasma-treated photocatalyst has also been utilized in photochemical water oxidation. The photoelectrochemical water splitting activity was evaluated with the plasma-treated (MPCVD system) nitrogen and hydrogen-doped mesoporous TiO_2 thin film [44,111]. Efficient separation of electron-hole pair separation, facile interfacial charge transfer, and high surface area were obtained by plasma-treated TiO_2, which significantly enhanced the water oxidation. Liu et al. (2021) assessed the photocatalytic activity of N-plasma-doped TiO_2 nanosheets. It was found that plasma-doped TiO_2 resulted in H_2 evolution 14.85 times greater than that of undoped TiO_2. The enhancement of photoactivity was due to oxygen vacancies and the reduction of Ti^{4+} to Ti^{3+} [112]. Yan et al. (2019) synthesized C-doped Co_3O_4 by CH_4 plasma and utilized the photocatalyst for water splitting. Plasma-assisted-sted incorporation of the C atom resulted in oxygen vacancies and substitution defects forming the Co-C bond. The Co-C bond and vacancies enhanced Hydrogen Evolution Reaction (HER) and Oxygen Evolution reaction (OER), respectively. In another study, Gholami et al. (2021) utilized a Magnetic WO_{3-x}-@Mesoporous carbon photocatalyst doped using N_2 plasma for enhanced H_2 production and antibiotic degradation. The H_2 evolution was found to be twice that of an undoped photocatalyst [87]. In a recent study, Wenwen Zhang et. al. (2020) reported the construction of an N-Cu_2O/CuO photocatalyst by N_2 plasma treating of Cu_2O octahedrons for H_2O_2 production under visible light [45]. The Cu_2O octahedron was placed in a plasma chamber (RF 13.56 MHz, 45 W) with an N_2 flow rate of 50 sccm and 100Pa. The

synthesized photocatalyst boosted the charge separation and transfer of photocurrent. The photocatalytic performance was dependent on plasma treatment time. The H_2O_2 generation of approximately 14 $\mu Mg^{-1}min^{-1}$ was achieved at 10 min of plasma treatment, which is 3 and 8 times more than Cu_2O and CuO, respectively. In one of the studies, Bello Ladan Muhammad et. al. (2021) investigated the optical properties of plasma-irradiated Fe-doped ZnO (Fe: ZnO) nanowires [113]. A CVD chamber was used with plasma power 500 W for 10 min. The plasma treatment increased the photoconductivity of the Fe: ZnO nanowires and the presence of a high density of shallow donor states were identified. **Table 4** summarizes different plasma-doped photocatalysts utilized for energy and other applications [44, 45, 71, 87, 111-113].

These studies suggest that the plasma-based process is a versatile technique for doping a wide range of photocatalysts with enhanced photocatalytic activities for environmental and energy applications. The versatile plasma approach can be further applied to many other photocatalysts including SnO_2. To reveal the diverse applications of plasma-treated photocatalysts, continuous research is going on, which would unveil more interesting characteristics of the plasma-treated catalysts in the near future.

6. Conclusions and Future perspectives

Plasma-based doping of semiconductor photocatalysts was shown remarkable performances in band gap engineering and enhanced visible light absorption which was the major part of solar energy. Among various doping methods, plasma treatment offered significant advantages including high doping efficiency by producing highly reactive radicals, atoms, and species, process simplicity, ability to reduce band gap to a large extent, relatively low-temperature operation, maintaining nanostructure of the original

596 nanomaterials, ability to dope a wide range of photocatalysts and capability of operating in
597 both gas and liquid phases. The plasma-treated photocatalysts showed significantly higher
598 photocatalytic performance than the materials doped by other methods. Although significant
599 advances were made, there are still some knowledge gaps on various aspects of the plasma
600 doping process. More theoretical studies were needed to understand the mechanism of plasma
601 doping processes, the interaction of the plasma species with the materials, and the impact of
602 various process parameters using high-performance computational modeling and simulations.
603 Correlations between theoretical and experimental results were also needed to advance the
604 plasma doping process.

605 The photocatalytic activities of most of the photocatalysts developed by plasma
606 treatment were evaluated mostly by dye degradation such as methylene blue. However,
607 limited studies were performed on the real-life applications of those photocatalysts. Extensive
608 studies were essential to determine the potential applications of those photocatalysts in
609 environmental and energy industries. For example, photocatalysts could be applied to energy-
610 efficient wastewater treatment with emerging pollutants such as degradation of Microcystin-
611 LR and Perfluoroalkyl and Polyfluoroalkyl Substances (PFAS) using solar energy. Those
612 photocatalysts could be incorporated into porous membranes to develop continuous
613 photocatalytic membrane reactors as opposed to the currently practiced batch reactor for
614 wastewater treatment and environmental remediation.

615 These highly efficient photocatalysts also disclosed tremendous promise in harnessing
616 and conversion of solar energy into solar fuel. For example, clean and green hydrogen was
617 produced by water splitting using the visible light active plasma treated photocatalysts driven
618 by solar energy. The plasma-treated photocatalysts also played a critical role in industrial
619 decarbonization and mitigating global warming. The photocatalysts absorbed sunlight and

used it for solar fuel production by combining carbon dioxide and water into fuel such as methanol, ethanol, or formic acid.

Another non-traditional application of those photocatalysts could be solar desalination. The demand for clean water was grown rapidly due to population growth, enhanced energy usage, and climate change. According to a World Bank report published in 2019, nearly half of the World's population experienced water scarcity every year. This dire water crisis in many water-scarce areas could be mitigated by producing clean water from inland and local brackish water sources due to its low salinity and widespread availability. Utilization of carbon-neutral renewable energy such as solar energy could be a novel approach for energy-efficient and potentially cost-effective desalination. Solar energy could be harnessed by plasma-treated photocatalysts for desalination by photo-electrodialysis process. In the photo-electrodialysis cell, a photoanode/photocatalyst absorbed the sunlight and produces electrons and holes. The excited holes oxidized water to produce oxygen gas and hydrogen ions. On the other hand, the excited electrons moved from the anode to the cathode, and reduce water to produce hydrogen gas and hydroxide ion which combined with the sodium ion of saline water to produce sodium hydroxide. Overall, clean water was produced from the saline water with the generation of hydrogen gas and sodium hydroxide.

Comprehensive research and development were critical for the development of energy-efficient, cost-effective, and scalable processes for industrial implementation of those advanced solar materials. Finally, techno-economic analysis and life cycle assessment were essential to evaluate the commercial viability and environmental sustainability of those promising solar materials.

For in-depth understanding, modeling is an efficient approach to simulate the plasma doping process. However, most of the studies in this field deal with plasma fluid modeling and there was very limited research reporting the in-situ modeling of a plasma doping process

and its correlation with the photocatalytic characteristics. The interactions of radicals/atoms/particles with metal oxide photocatalysts have not received attention yet [114]. The molecular dynamics simulation (MD) approach for understanding the doping process and its impact on the photocatalytic nature should be studied to obtain an in-depth knowledge of the plasma doping process.

Acknowledgments

The authors acknowledge the support from Curtin University, Australia, and Laboratory Directed Research and Development Fund, Oak Ridge National Laboratory, USA.

References

[1] G.H. Al-Hazmi, M.S. Refat, K.F. Alshammari, K.T. Kubra, A. Shahat, Efficient toxic doxorubicin hydrochloride removal from aqueous solutions using facial alumina nanorods, J. Mol. Struct. 1272 (2023) 134187.

[2] Q. Guo, C. Zhou, Z. Ma, X. Yang, Fundamentals of TiO2 Photocatalysis: Concepts, Mechanisms, and Challenges, Adv. Mater. 31 (2019) 1901997.

[3] K.T. Kubra, M.S. Salman, M.N. Hasan, Enhanced toxic dye removal from wastewater using biodegradable polymeric natural adsorbent, J. Mol. Liq. 328 (2021) 115468.

[4] M.S. Salman, M.C. Sheikh, M.M. Hasan, M.N. Hasan, K.T. Kubra, A.I. Rehan, A.I. Rasee, R.M. Waliullah, M.S. Hossain, M.A. Khaleque, A.K.D. Alsukaibi, H.M. Alshammari, Chitosan-coated cotton fiber composite for efficient toxic dye encapsulation from aqueous media, Appl. Surf. Sci. 622 (2023) 157008.

668 [5] K.T. Kubra, M.M. Hasan, M.N. Hasan, M.S. Salman, M.C. Sheikh, A.I. Rehan, A.I.
669 Rasee, R.M. Waliullah, M.S. Hossain, A.K.D. Alsukaibi, H.M. Alshammari, The
670 heavy lanthanide of Thulium(III) separation and recovery using specific ligand-based
671 facial composite adsorbent, Colloid. Surface. A 667 (2023) 131415.

672 [6] K.T. Kubra, M.S. Salman, H. Znad, M.N. Hasan, Efficient encapsulation of toxic dye
673 from wastewater using biodegradable polymeric adsorbent, J. Mol. Liq. 329 (2021)
674 115541.

675 [7] A. Shahat, K.T. Kubra, M.S. Salman, M.N. Hasan, M.M. Hasan, Novel solid-state
676 sensor material for efficient cadmium(II) detection and capturing from wastewater,
677 Microchem. J. 164 (2021) 105967.

678 [8] M.S. Salman, M.N. Hasan, M.M. Hasan, K.T. Kubra, M.C. Sheikh, A.I. Rehan, R.M.
679 Waliullah, A.I. Rasee, M.S. Hossain, A.K.D. Alsukaibi, H.M. Alshammari, Improving
680 copper(II) ion detection and adsorption from wastewater by the ligand-functionalized
681 composite adsorbent, J. Mol. Struct. 1282 (2023) 135259.

682 [9] C. Bie, H. Yu, B. Cheng, W. Ho, J. Fan, J. Yu, Design, Fabrication, and Mechanism of
683 Nitrogen-Doped Graphene-Based Photocatalyst, Adv. Mater. 33 (2021) 2003521.

684 [10] M.N. Hasan, M.S. Salman, M.M. Hasan, K.T. Kubra, M.C. Sheikh, A.I. Rehan, A.I.
685 Rasee, R.M. Waliullah, M.S. Hossain, A. Islam, S. Khandaker, A.K.D. Alsukaibi,
686 H.M. Alshammari, Assessing sustainable Lutetium(III) ions adsorption and recovery
687 using novel composite hybrid nanomaterials, J. Mol. Struct. 1276 (2023) 134795.

688 [11] M.M. Hasan, K.T. Kubra, M.N. Hasan, M.S. Salman, M.C. Sheikh, A.I. Rehan, A.I.
689 Rasee, R.M. Waliullah, M.S. Islam, S. Khandaker, A. Islam, M.S. Hossain, A.K.D.
690 Alsukaibi, H.M. Alshammari, Sustainable ligand-modified based composite material

for the selective and effective cadmium(II) capturing from wastewater, J. Mol. Liq. 371 (2023) 121125.

[12] D. Huang, G. Wang, M. Cheng, G. Zhang, S. Chen, Y. Liu, Z. Li, W. Xue, L. Lei, R. Xiao, Optimal preparation of catalytic Metal-organic framework derivatives and their efficient application in advanced oxidation processes, Chem. Eng. J. 421 (2021) 127817.

[13] R. Shwetharani, H.R. Chandan, M. Sakar, G.R. Balakrishna, K.R. Reddy, A. V. Raghu, Photocatalytic semiconductor thin films for hydrogen production and environmental applications, Int. J. Hydrogen Energy. 45 (2020) 18289–18308.

[14] M.M. Rahman, Selective capturing of phenolic derivative by a binary metal oxide microcubes for its detection, Sci. Reports 2019 91. 9 (2019) 1–10.

[15] G. Wang, D. Huang, M. Cheng, S. Chen, G. Zhang, L. Du, L. Lei, Y. Chen, R. Li, Y. Liu, An insight into the bridging role of Co3O4 in MOF-derived binary metal oxide modified sheet-like g-C3N4 for photo-assisted peroxymonosulfate activation, Environ. Sci. Nano. 384 (2022) 4393–4410.

[16] C. Zhou, W. Xia, D. Huang, M. Cheng, H. Zhang, T. Cai, W. Xiong, Y. Yang, B. Song, W. Wang, M. Zhou, G. Zeng, Strategies for enhancing the perylene diimide photocatalytic degradation activity: method, effect factor, and mechanism, Environ. Sci. Nano. 8 (2021) 602–618.

[17] M.S. Salman, M.N. Hasan, K.T. Kubra, M.M. Hasan, Optical detection and recovery of Yb(III) from waste sample using novel sensor ensemble nanomaterials, Microchem. J. 162 (2021) 105868.

[18] H. Liu, W. Guo, Y. Li, S. He, C. He, Photocatalytic degradation of sixteen organic

dyes by TiO2/WO3-coated magnetic nanoparticles under simulated visible light and solar light, J. Environ. Chem. Eng. 6 (2018) 59–67.

[19] M.N. Hasan, M.S. Salman, A. Islam, H. Znad, M.M. Hasan, Sustainable composite sensor material for optical cadmium(II) monitoring and capturing from wastewater, Microchem. J. 161 (2021) 105800.

[20] P. Devendran, D. Selvakumar, G. Ramadoss, R. Sivaramakrishnan, T. Alagesan, R. Jayavel, K. Pandian, A novel visible light active rare earth doped CdS nanoparticles decorated reduced graphene oxide sheets for the degradation of cationic dye from wastewater, Chemosphere. 287 (2022) 132091.

[21] X. Sun, L. Shi, Q. Bai, Z. Yin, H. Song, X. Qu, Synthesis of BiOCl/Bi3NbO7 heterojunction by in-situ chemical etching with enhanced photocatalytic performance for the degradation of organic pollutants, Appl. Surf. Sci. 587 (2022) 152633.

[22] M.R. Al-Mamun, M.S. Islam, M.R. Hossain, S. Kader, M.S. Islam, M.Z.H. Khan, A novel and highly efficient Ag and GO co-synthesized ZnO nano photocatalyst for methylene blue dye degradation under UV irradiation, Environ. Nanotechnology, Monit. Manag. 16 (2021) 100495.

[23] V.K. Mrunal, A.K. Vishnu, N. Momin, J. Manjanna, Cu2O nanoparticles for adsorption and photocatalytic degradation of methylene blue dye from aqueous medium, Environ. Nanotechnology, Monit. Manag. 12 (2019) 100265.

[24] P. Xu, M. Chen, C. Lai, G. Zeng, D. Huang, H. Wang, X. Gong, L. Qin, Y. Liu, D. Mo, X. Wen, C. Zhou, R. Wang, Effects of typical engineered nanomaterials on 4-nonylphenol degradation in river sediment: based on bacterial community and function analysis, Environ. Sci.: Nano, 6 (2019) 2171-2184.

737 [25] M.M. Rahman, A. Jamal, S.B. Khan, M. Faisal, Highly sensitive ethanol chemical
738 sensor based on Ni-doped SnO_2 nanostructure materials, Biosens. Bioelectron. 28
739 (2011) 127–134.

740 [26] (a) G. Abdulkareem-Alsultan, N. Asikin-Mijan, H. V. Lee, U. Rashid, A. Islam, Y. H.
741 Taufiq-Yap, A review on thermal conversion of plant oil (edible and inedible) into
742 green fuel using carbon-based nanocatalyst, Catalysts 9 (2019) 350;

743 (b) K. L. Theam, A. Islam, Y. M. Choo, Y. H. Taufiq-Yap, Biodiesel from low cost palm
744 stearin using metal doped methoxide solid catalyst. Ind. Crops Prod. 76 (2015) 281-
745 289.

746 [27] K.P.O. Mahesh, D.H. Kuo, Synthesis of Ni nanoparticles decorated SiO2/TiO2
747 magnetic spheres for enhanced photocatalytic activity towards the degradation of azo
748 dye, Appl. Surf. Sci. 357 (2015) 433–438.

749 [28] B.M. Pirzada, O. Mehraj, S.A. Bhat, S. Sabir, Efficient visible-light-driven
750 Photocatalytic activity and enhanced charge transfer properties over Mo-doped
751 WO3/TiO2 nanocomposites, J. Environ. Chem. Eng. 6 (2018) 3204–3212.

752 [29] X. Qu, S. Hu, J. Bai, P. Li, G. Lu, X. Kang, A facile approach to synthesize oxygen
753 doped g-C3N4 with enhanced visible light activity under anoxic conditions: Via
754 oxygen-plasma treatment, New J. Chem. 42 (2018) 4998–5004.

755 [30] Y. Liu, Y. Deng, Z. Sun, J. Wei, G. Zheng, A.M. Asiri, S.B. Khan, M.M. Rahman, D.
756 Zhao, Hierarchical Cu2S microsponges constructed from nanosheets for efficient
757 photocatalysis, Small. 9 (2013) 2702–2708.

758 [31] G. Yang, T. Wang, B. Yang, Z. Yan, S. Ding, T. Xiao, Enhanced visible-light activity
759 of F-N co-doped TiO 2 nanocrystals via nonmetal impurity, Ti3+ ions and oxygen

760 vacancies, Appl. Surf. Sci. 287 (2013) 135–142.

761 [32] X. Wang, L.L. Wang, D. Guo, L.L. Ma, B.L. Zhu, P. Wang, G.C. Wang, S.M. Zhang,
762 W.P. Huang, Fabrication and photocatalytic performance of C, N, F-tridoped TiO 2
763 nanotubes, Catal. Today. 327 (2019) 182–189.

764 [33] M.M. Rahman, A.M. Asiri, T.E. Youssef, H.M. Marwani, Photocatalytic degradation
765 of remazol brilliant orange 3R using wet-chemically prepared CdO-ZnO nanofibers for
766 environmental remediation, Mater. Express. 6 (2016) 137–148.

767 [34] (a) S.I.S. Mashuri, M.L. Ibrahim, M.F. Kasim, M.S. Mastuli, U. Rashid, A.H.
768 Abdullah, A. Islam, N. Asikin Mijan, Y.H. Tan, N. Mansir, N.H.M Kaus,
769 Photocatalysis for organic wastewater treatment: From the basis to current challenges
770 for society. Catalysts, 10 (2020) 1260;

771 (b) A. Islam, Y.H. Taufiq-Yap, C.M. Chu, E.S. Chan, P. Ravindra, Synthesis and
772 characterization of millimetric gamma alumina spherical particles by oil drop
773 granulation method. J. Porous Mater. 19 (2012) 807-817.

774 [35] M.R. Al-Mamun, S. Kader, M.S. Islam, M.Z.H. Khan, Photocatalytic activity
775 improvement and application of UV-TiO2 photocatalysis in textile wastewater
776 treatment: A review, J. Environ. Chem. Eng. 7 (2019) 103248.

777 [36] M.M. Rahman, J. Ahmed, A.M. Asiri, Thiourea sensor development based on
778 hydrothermally prepared CMO nanoparticles for environmental safety, Biosens.
779 Bioelectron. 99 (2018) 586–592.

780 [37] M.M. Rahman, J. Ahmed, A.M. Asiri, Development of Creatine sensor based on
781 antimony-doped tin oxide (ATO) nanoparticles, Sensor. Actuat. B: Chem. 242 (2017)
782 167–175.

783 [38] M.R. Al-Mamun, K.T. Hossain, S. Mondal, M.A. Khatun, M.S. Islam, D.M.Z.H.
784 Khan, Synthesis, characterization, and photocatalytic performance of methyl orange in
785 aqueous TiO2 suspension under UV and solar light irradiation, South African J. Chem.
786 Eng. 40 (2022) 113–125.

787 [39] (a) E.S. Chan, T.K. Lim, P. Ravindra, R.F. Mansa, A. Islam, The effect of low air-to-
788 liquid mass flow rate ratios on the size, size distribution and shape of calcium alginate
789 particles produced using the atomization method. J. Food Eng. 108 (2012) 297-303;

790 (b) K. N. Islam, M.Z.B.A. Ali, M. Y. Bakar, A. Loqman, M. S. Islam, A. Islam, M. Ullah, A
791 novel catalytic method for the synthesis of spherical aragonite nanoparticles from
792 cockle shells, Powder Technol. 246 (2013) 434-440.

793 [40] J. Sun, L. Qiao, S. Sun, G. Wang, Photocatalytic degradation of Orange G on nitrogen-
794 doped TiO2 catalysts under visible light and sunlight irradiation, J. Hazard. Mater. 155
795 (2008) 312–319.

796 [41] C. Sarantopoulos, A.N. Gleizes, F. Maury, Chemical vapor deposition and
797 characterization of nitrogen doped TiO2 thin films on glass substrates, Thin Solid
798 Films. 518 (2009) 1299–1303.

799 [42] (a) S.H. Teo, A. Islam, C.H. Ng, N. Mansir, T. Ma, S. T. Choong, Y.H. Taufiq-Yap,
800 Methoxy-functionalized mesostructured stable carbon catalysts for effective biodiesel
801 production from non-edible feedstock, Chem. Eng. J. 334 (2018)1851-1868;

802 (b) S.H. Teo, A. Islam, H.R.F. Masoumi, Y.H. Taufiq-Yap, J. Janaun, E.S. Chan, Effective
803 synthesis of biodiesel from Jatropha curcas oil using betaine assisted nanoparticle
804 heterogeneous catalyst from eggshell of Gallus domesticus, Renewable Energy, 111
805 (2017) 892-905.

[43] M.M. Rahman, J. Ahmed, Cd-doped Sb2O4 nanostructures modified glassy carbon electrode for efficient detection of melamine by electrochemical approach, Biosens. Bioelectron. 102 (2018) 631–636.

[44] S.Z. Islam, A. Reed, N. Wanninayake, D.Y. Kim, S.E. Rankin, Remarkable Enhancement of Photocatalytic Water Oxidation in N2/Ar Plasma Treated, Mesoporous TiO2 Films, J. Phys. Chem. C. 120 (2016) 14069–14081.

[45] W. Zhang, X. Chen, X. Zhao, M. Yin, L. Feng, H. Wang, Simultaneous nitrogen doping and Cu2O oxidization by one-step plasma treatment toward nitrogen-doped Cu2O@CuO heterostructure: An efficient photocatalyst for H2O2 evolution under visible light, Appl. Surf. Sci. 527 (2020) 146908.

[46] M.S. Salman, H. Znad, M.N. Hasan, M.M. Hasan, Optimization of innovative composite sensor for Pb(II) detection and capturing from water samples, Microchem. J. 160 (2021) 105765.

[47] J. Ding, X. Sun, Q. Wang, D. sheng Li, X. Li, X. Li, L. Chen, X. Zhang, X. Tian, K. (Ken) Ostrikov, Plasma synthesis of Pt/g-C3N4 photocatalysts with enhanced photocatalytic hydrogen generation, J. Alloys Compd. 873 (2021) 159871.

[48] (a) A. Islam, S. H. Teo, M. T. Ahmed, S. Khandaker, M. L. Ibrahim, D. V. N. Vo, A. S. Khan, Novel micro-structured carbon-based adsorbents for notorious arsenic removal from wastewater, Chemosphere, 272 (2021) 29653;

(b) L. F. How, A. Islam, M. S. Jaafar, Y. H. Taufiq-Yap, Extraction and characterization of γ-alumina from waste aluminium dross, Waste Biomass Valorization 8 (2017) 321-327.

[49] A. Ramos-Corona, R. Rangel, J. Lara-Romero, A. Ramos-Carrazco, Nitrogen-plasma doped ZnO-graphene oxide compounds production and their photocatalytic

829 performance, Adv. Powder Technol. 33 (2022) 103829.

830 [50] Y. Yan, M. Han, A. Konkin, T. Koppe, D. Wang, T. Andreu, G. Chen, U. Vetter, J.R.
831 Morante, P. Schaaf, Slightly hydrogenated TiO2 with enhanced photocatalytic
832 performance, J. Mater. Chem. A. 2 (2014) 12708–12716.

833 [51] W. Bootluck, T. Chittrakarn, K. Techato, W. Khongnakorn, Modification of surface α-
834 Fe2O3/TiO2 photocatalyst nanocomposite with enhanced photocatalytic activity by Ar
835 gas plasma treatment for hydrogen evolution, J. Environ. Chem. Eng. 9 (2021) 105660.

836 [52] M.R. Awual, M.N. Hasan, M.M. Hasan, M.S. Salman, M.C. Sheikh, K.T. Kubra, M.S.
837 Islam, H.M. Marwani, A. Islam, M.A. Khaleque, R.M. Waliullah, M.S. Hossain, A.I.
838 Rasee, A.I. Rehan, M.E. Awual, Green and robust adsorption and recovery of
839 Europium(III) with a mechanism using hybrid donor conjugate materials, Sep. Purif.
840 Technol. (2023) 124088. https://doi.org/10.1016/j.seppur.2023.124088

841 [53] B. Pant, M. Park, S.J. Park, Recent advances in TiO2 films prepared by sol-gel
842 methods for photocatalytic degradation of organic pollutants and antibacterial
843 activities, Coatings. 9 (2019) 1–19.

844 [54] K.M. Sandhya, L.T. Manamel, B.C. Das, Doping of Semiconductors at Nanoscale with
845 Microwave Heating (Overview), Microw. Heat. Electromagn. Fields Causing Therm.
846 Non-Thermal Eff. (2021) 81.

847 [55] H. Li, Y. Hao, H. Lu, L. Liang, Y. Wang, J. Qiu, X. Shi, Y. Wang, J. Yao, A
848 systematic study on visible-light N-doped TiO2 photocatalyst obtained from
849 ethylenediamine by sol–gel method, Appl. Surf. Sci. 344 (2015) 112–118.

850 [56] L.D. Than, N.S. Luong, V.D. Ngo, N.M. Tien, T.N. Dung, N.M. Nghia, N.T. Loc,
851 V.T. Thu, T.D. Lam, Highly visible light activity of nitrogen doped TiO2 prepared by

852 sol–gel approach, J. Electron. Mater. 46 (2017) 158–166.

853 [57] S.Z. Islam, S.E. Rankin, Hydrazine-based synergistic Ti(III)/N doping of surfactant-
854 templated TiO2 thin films for enhanced visible light photocatalysis, Mater. Chem.
855 Phys. 182 (2016) 382–393.

856 [58] S.Z. Islam, A. Reed, D.Y. Kim, S.E. Rankin, N2/Ar plasma induced doping of ordered
857 mesoporous TiO2 thin films for visible light active photocatalysis, Microporous
858 Mesoporous Mater. 220 (2016) 120–128.

859 [59] M. Russo, G. Iervolino, V. Vaiano, V. Palma, Non-Thermal Plasma Coupled with
860 Catalyst for the Degradation of Water Pollutants: A Review, Catal. 2020, Vol. 10,
861 Page 1438. 10 (2020) 1438.

862 [60] S. Li, X. Dang, X. Yu, G. Abbas, Q. Zhang, L. Cao, The application of dielectric
863 barrier discharge non-thermal plasma in VOCs abatement: A review, Chem. Eng. J.
864 388 (2020) 124275.

865 [61] P. Murugesan, V. Evanjalin Monica, J.A. Moses, C. Anandharamakrishnan, Water
866 decontamination using non-thermal plasma: Concepts, applications, and prospects, J.
867 Environ. Chem. Eng. 8 (2020) 104377.

868 [62] Z. Ye, L. Zhao, A. Nikiforov, J.M. Giraudon, Y. Chen, J. Wang, X. Tu, A review of
869 the advances in catalyst modification using nonthermal plasma: Process, Mechanism
870 and Applications, Adv. Colloid Interface Sci. 308 (2022) 102755.

871 [63] A. Indarto, J.-W. Choi, H. Lee, H.K. Song, Decomposition of greenhouse gases by
872 plasma, Environ. Chem. Lett. 6 (2008) 215–222.

873 [64] P. Dong, X. Cheng, Z. Jin, Z. Huang, X. Nie, X. Wang, X. Zhang, The green synthesis

of Ag-loaded photocatalyst via DBD cold plasma assisted deposition of Ag nanoparticles on N-doped TiO2 nanotubes, J. Photochem. Photobiol. A Chem. 382 (2019) 111971.

[65] W. Zhao, S. Liu, S. Zhang, R. Wang, K. Wang, Preparation and visible-light photocatalytic activity of N-doped TiO2 by plasma-assisted sol-gel method, Catal. Today. 337 (2019) 37–43.

[66] M. Zhou, Novel photocatalytic TiO2-based porous membranes prepared by plasma-enhanced chemical vapor deposition (PECVD) for organic pollutant degradation in water, University of Montpellier, University of Chemistry and Technology, Prague (UCTP), University of Calabria, Rende, 2015.

[67] Q. Chen, A. Ozkan, B. Chattopadhyay, K. Baert, C. Poleunis, A. Tromont, R. Snyders, A. Delcorte, H. Terryn, M.P. Delplancke-Ogletree, Y.H. Geerts, F. Reniers, N-Doped TiO2 Photocatalyst Coatings Synthesized by a Cold Atmospheric Plasma, Langmuir. 35 (2019) 7161–7168.

[68] A. Fateev, F. Leipold, Y. Kusano, B. Stenum, E. Tsakadze, H. Bindslev, Plasma chemistry in an atmospheric pressure Ar/NH3 dielectric barrier discharge, Plasma Process. Polym. 2 (2005) 193–200.

[69] Z.S. Chang, C.W. Yao, S. Le Chen, G.J. Zhang, Electrical and optical properties of Ar/NH3 atmospheric pressure plasma jet, Phys. Plasmas. 23 (2016) 093503.

[70] A. Sarani, A.Y. Nikiforov, C. Leys, Atmospheric pressure plasma jet in Ar and Ar/H2O mixtures: Optical emission spectroscopy and temperature measurements, Phys. Plasmas. 17 (2010) 063504.

[71] D. Yan, R. Chen, Z. Xiao, S. Wang, Engineering the electronic structure of Co3O4 by

carbon-doping for efficient overall water splitting, Electrochim. Acta. 303 (2019) 316–322.

[72] L. Hao, H. Huang, Y. Zhang, T. Ma, Oxygen Vacant Semiconductor Photocatalysts, Adv. Funct. Mater. 31 (2021).

[73] G. Li, R. Huang, C. Zhu, G. Jia, S. Zhang, Q. Zhong, Effect of oxygen vacancies and its quantity on photocatalytic oxidation performance of titanium dioxide for NO removal, Colloids Surfaces A Physicochem. Eng. Asp. 614 (2021) 126156.

[74] Y. Huang, Y. Yu, Y. Yu, B. Zhang, Oxygen Vacancy Engineering in Photocatalysis, Sol. RRL. 4 (2020) 2000037.

[75] G. Zhuang, Y. Chen, Z. Zhuang, Y. Yu, J. Yu, Oxygen vacancies in metal oxides: recent progress towards advanced catalyst design, Sci. China Mater. 63 (2020) 2089–2118.

[76] J. Sengupta, Carbon Nanotube Fabrication at Industrial Scale: Opportunities and Challenges, Handb. Nanomater. Ind. Appl. (2018) 172–194.

[77] G.W. Ho, A.T.S. Wee, J. Lin, W.C. Tjiu, Synthesis of well-aligned multiwalled carbon nanotubes on Ni catalyst using radio frequency plasma-enhanced chemical vapor deposition, Thin Solid Films. 388 (2001) 73–77.

[78] V. Teixeira, J. Carneiro, P. Carvalho, E. Silva, S. Azevedo, C. Batista, High barrier plastics using nanoscale inorganic films, in: Multifunct. Nanoreinforced Polym. Food Packag., Woodhead Publishing, 2011: pp. 285–315.

[79] F. Kruger, M.J. Kushner, S. Shim, H. Lee, S.-K. Nam, ICP vs CCP in High Aspect Ratio Etching of SiO 2 using Ar/C 4 F 8 /O 2 Gas Mixtures, in: 2020 IEEE Int. Conf.

Plasma Sci., Institute of Electrical and Electronics Engineers (IEEE), 2020: pp. 88–88.

[80] B. Liu, L. Wen, X. Zhao, The structure and photocatalytic studies of N-doped TiO2 films prepared by radio frequency reactive magnetron sputtering, Sol. Energy Mater. Sol. Cells. 92 (2008) 1–10.

[81] F. Shi, Introductory Chapter: Basic Theory of Magnetron Sputtering, Magnetron Sputtering [Working Title]. (2018).

[82] G. Shivkumar, S.S. Tholeti, M.A. Alrefae, T.S. Fisher, A.A. Alexeenko, Analysis of hydrogen plasma in a microwave plasma chemical vapor deposition reactor, J. Appl. Phys. 119 (2016) 113301.

[83] W. Ahmed, H. Sein, M. Jackson, C. Rego, I.U. Hassan, K. Subramani, J. Yazdani, Surface Engineering of Dental Tools with Diamond for Improved Life and Performance, Emerg. Nanotechnologies Dent. (2012) 239–272.

[84] Y. Liu, J. He, N. Zhang, W. Zhang, Y. Zhou, K. Huang, Advances of microwave plasma-enhanced chemical vapor deposition in fabrication of carbon nanotubes: a review, J. Mater. Sci. 56 (2021) 12559–12583.

[85] P. Kalra, Advanced Source/drain Technologies for Nanoscale CMOS., University of California, Berkeley, 2008. http://books.google.com/books?hl=en&lr=&id=PX-nWeUN-xsC&oi=fnd&pg=PA1&dq=Advanced+Source/Drain+Technologies+for+nanoscale+CMOS&ots=TkB1cCcPuB&sig=4RlYL69iBwWTOrACG9sHacJlA6g (accessed July 30, 2022).

[86] M. Roy, Protective Hard Coatings for Tribological Applications, Mater. Under Extrem. Cond. Recent Trends Futur. Prospect. (2017) 259–292.

[87] P. Gholami, A. Khataee, A. Bhatnagar, B. Vahid, Synthesis of N-Doped Magnetic WO3- x@Mesoporous Carbon Using a Diatom Template and Plasma Modification: Visible-Light-Driven Photocatalytic Activities, ACS Appl. Mater. Interfaces. 13 (2021) 13072–13086.

[88] S. Roy, B. Choudhury, J. Johnson, A. Schindler-Tyka, Application of dielectric barrier discharge for improving food shelf life and reducing spoilage, Sci. Reports 2021 111. 11 (2021) 1–9.

[89] J. He, X. Wen, L. Wu, H. Chen, J. Hu, X. Hou, Dielectric barrier discharge plasma for nanomaterials: Fabrication, modification and analytical applications, TrAC Trends Anal. Chem. 156 (2022) 116715.

[90] T. Zhu, S. Li, B. Ren, L. Zhang, L. Dong, L. Tan, Plasma-induced synthesis of boron and nitrogen co-doped reduced graphene oxide for super-capacitors, J. Mater. Sci. 54 (2019) 9632–9642.

[91] S. Hu, F. Li, Z. Fan, J. Gui, The effect of H2–CCl4 mixture plasma treatment on TiO2 photocatalytic oxidation of aromatic air contaminants under both UV and visible light, Chem. Eng. J. 236 (2014) 285–292.

[92] L. Ma, S. Hu, P. Li, Q. Wang, H. Ma, W. Li, L. Ma, S. Hu, P. Li, Q. Wang, H. Ma, W. Li, In situ synthesis of sulfur doped carbon nitride with enhanced photocatalytic performance using DBD plasma treatment under H₂S atmosphere, JPCS. 118 (2018) 166–171.

[93] L. Tao, X. Duan, C. Wang, X. Duan, S. Wang, Plasma-engineered MoS2 thin-film as an efficient electrocatalyst for hydrogen evolution reaction, Chem. Commun. 51 (2015) 7470–7473.

965 [94] H. Lee, B.J. Kim, Y.K. Park, J.S. Kim, S.C. Jung, Assessment of photocatalytic
966 performance of Fe/N-TiO2 photocatalysts prepared by liquid phase plasma process,
967 Catal. Today. 355 (2020) 435–442.

968 [95] H. Lee, S.H. Park, S.J. Kim, Y.K. Park, B.H. Kim, S.C. Jung, Synthesis of tin and tin
969 oxide nanoparticles using liquid phase plasma in an aqueous solution, Microelectron.
970 Eng. 126 (2014) 153–157.

971 [96] H. Lee, S.H. Park, S.J. Kim, Y.K. Park, B.J. Kim, K.H. An, S.J. Ki, S.C. Jung,
972 Synthesis of manganese oxide/activated carbon composites for supercapacitor
973 application using a liquid phase plasma reduction system, Int. J. Hydrogen Energy. 40
974 (2015) 754–759.

975 [97] S.H. Sun, S.C. Jung, Facile synthesis of bimetallic Ni-Cu nanoparticles using liquid
976 phase plasma method, Korean J. Chem. Eng. 2016 333. 33 (2016) 1075–1079.

977 [98] S. Horikoshi, N. Serpone, In-liquid plasma: a novel tool in the fabrication of
978 nanomaterials and in the treatment of wastewaters, RSC Adv. 7 (2017) 47196–47218.

979 [99] Q. Chen, J. Li, Y. Li, A review of plasma-liquid interactions for nanomaterial
980 synthesis, J. Phys. D. Appl. Phys. 48 (2015).

981 [100] P.J. Boruah, P. Kalita, H. Bailung, In-Liquid Plasma: A Novel Tool for
982 Nanofabrication, in: Plasma Sci. Technol., IntechOpen, 2021.

983 [101] W.G. Graham, K.R. Stalder, Plasmas in liquids and some of their applications in
984 nanoscience, J. Phys. D. Appl. Phys. 44 (2011) 174037.

985 [102] S. Horikoshi, S. Sato, M. Abe, N. Serpone, A novel liquid plasma AOP device
986 integrating microwaves and ultrasounds and its evaluation in defluorinating

perfluorooctanoic acid in aqueous media, Ultrason. Sonochem. 18 (2011) 938–942.

[103] S.C. Jung, H.J. Bang, H. Lee, H.H. Ha, Y.H. Yu, S.J. Kim, Y.K. Park, Assessing the photocatalytic activity of europium doped TiO2 using liquid phase plasma process on acetylsalicylic acid, Catal. Today. 388–389 (2022) 365–371.

[104] S.J. Ki, Y.K. Park, J.S. Kim, W.J. Lee, H. Lee, S.C. Jung, Facile preparation of tungsten oxide doped TiO2 photocatalysts using liquid phase plasma process for enhanced degradation of diethyl phthalate, Chem. Eng. J. 377 (2019) 120087.

[105] H. Lee, Y.K. Park, S.J. Kim, B.H. Kim, S.C. Jung, Fe-decorated TiO2 powder photocatalysts with enhanced visible-light-driven degradation activities, Surf. Coatings Technol. 307 (2016) 1018–1023.

[106] H. Lee, Y.-K. Park, S.-C. Jung, Preparation of N and Eu doped TiO2 using plasma in liquid process and its photocatalytic degradation activity for diclofenac, Korean J. Chem. Eng. 2022 398. 39 (2022) 2080–2088.

[107] H.U. Lee, Y.C. Lee, S.C. Lee, S.Y. Park, B. Son, J.W. Lee, C.H. Lim, C.J. Choi, M.H. Choi, S.Y. Lee, Y.K. Oh, J. Lee, Visible-light-responsive bicrystalline (anatase/brookite) nanoporous nitrogen-doped TiO2 photocatalysts by plasma treatment, Chem. Eng. J. 254 (2014) 268–275.

[108] P. Manojkumar, E. Lokeshkumar, A. Saikiran, B. Govardhanan, M. Ashok, N. Rameshbabu, Visible light photocatalytic activity of metal (Mo/V/W) doped porous TiO2 coating fabricated on Cp-Ti by plasma electrolytic oxidation, J. Alloys Compd. 825 (2020) 154092.

[109] C.Y. Tsai, H.C. Hsi, T.H. Kuo, Y.M. Chang, J.H. Liou, Preparation of Cu-doped TiO2 photocatalyst with thermal plasma torch for low-concentration mercury removal,

1010 Aerosol Air Qual. Res. 13 (2013) 639–648.

1011 [110] L. Zhang, L. Feng, P. Li, X. Chen, Y. Gao, Y. Gong, Z. Du, S. Zhang, A. Zhang, G.
1012 Chen, H. Wang, Plasma-assisted doping of nitrogen into cobalt sulfide for loading
1013 cadmium sulfide: A direct Z-scheme heterojunction for efficiently photocatalytic
1014 Cr(VI) reduction under visible light, Chem. Eng. J. 417 (2021) 129222.

1015 [111] S.Z. Islam, A. Reed, S. Nagpure, N. Wanninayake, J.F. Browning, J. Strzalka, D.Y.
1016 Kim, S.E. Rankin, Hydrogen incorporation by plasma treatment gives mesoporous
1017 black TiO2 thin films with visible photoelectrochemical water oxidation activity,
1018 Microporous Mesoporous Mater. 261 (2018) 35–43.

1019 [112] X. Liu, R. Hua, J. Niu, Z. Zhang, J. Zhang, N2 plasma treatment TiO2 nanosheets for
1020 enhanced visible light-driven photocatalysis, J. Alloys Compd. 881 (2021) 160509.

1021 [113] B. Ladan Muhammad, F. Cummings, Nitrogen plasma irradiation of Fe doped ZnO
1022 nanowire arrays for improved optical properties, Mater. Today Proc. 36 (2019) 383–
1023 389.

1024 [114] S. Vepřek, Plasma-induced and plasma-assisted chemical vapour deposition, Thin
1025 Solid Films. 130 (1985) 135–154.

1026 [115] H.O. Pierson, Handbook of chemical vapor deposition : principles, technology, and
1027 applications, 2nd ed., Noyes Publications, 1999.

1028 [116] B. Pant, M. Park, S.-J. Park, Recent advances in TiO2 films prepared by sol-gel
1029 methods for photocatalytic degradation of organic pollutants and antibacterial
1030 activities, Coatings. 9 (2019) 613.

1031 [117] K. Rajendran, V.S. Kumar, K.A. Rani, Synthesis and characterization of immobilized

activated carbon doped TiO2 thin films, Optik (Stuttg). 125 (2014) 1993–1996.

[118] Z.N. Kayani, S. Riaz, Magnetic and antibacterial studies of sol-gel dip coated Ce doped TiO2 thin films: Influence of Ce contents, Ceram. Int. 46 (2020) 381–390.

[119] S. Obregón, V. Rodríguez-González, Photocatalytic TiO2 thin films and coatings prepared by sol–gel processing: a brief review, J. Sol-Gel Sci. Technol. (2021) 1–17.

[120] P.M. Wilson, G.N. Mbah, T.G. Smith, D. Schmidt, R.Y. Lai, T. Hofmann, A. Sinitskii, Three-dimensional periodic graphene nanostructures, J. Mater. Chem. C. 2 (2014) 1879–1886.

[121] V.K. Yemmireddy, Y. Hung, Using photocatalyst metal oxides as antimicrobial surface coatings to ensure food safety—Opportunities and challenges, Compr. Rev. Food Sci. Food Saf. 16 (2017) 617–631.

[122] J. Liu, H. Liu, X. Zuo, F. Wen, H. Jiang, H. Cao, Y. Pei, Micro-patterned TiO2 films for photocatalysis, Mater. Lett. 254 (2019) 448–451.

[123] D. Mardare, F. Iacomi, N. Cornei, M. Girtan, D. Luca, Undoped and Cr-doped TiO2 thin films obtained by spray pyrolysis, Thin Solid Films. 518 (2010) 4586–4589.

[124] G. Varshney, S.R. Kanel, D.M. Kempisty, V. Varshney, A. Agrawal, E. Sahle-Demessie, R.S. Varma, M.N. Nadagouda, Nanoscale TiO2 films and their application in remediation of organic pollutants, Coord. Chem. Rev. 306 (2016) 43–64.

[125] K. Wetchakun, N. Wetchakun, S. Sakulsermsuk, An overview of solar/visible light-driven heterogeneous photocatalysis for water purification: TiO2-and ZnO-based photocatalysts used in suspension photoreactors, J. Ind. Eng. Chem. 71 (2019) 19–49.

[126] M. Sarmadi, Advantages and disadvantages of plasma treatment of textile materials,

in: 21st Int. Symp. Plasma Chem. (ISPC 21), Sunday, 2013.

[127] S. Hosseini, A. Amoozadeh, Plasma treatment as a promising environmentally benign approach for synthesis of valuable multi-gas doped nano-TiO2-P25: An efficient way to boost the photocatalytic performance under visible light illumination, Photochem. Photobiol. 97 (2021) 672–687.

[128] Y. Hamedani, P. Macha, T.J. Bunning, R.R. Naik, M.C. Vasudev, Plasma-Enhanced Chemical Vapor Deposition: Where we are and the Outlook for the Future, Chem. Vap. Depos. - Recent Adv. Appl. Opt. Sol. Cells Solid State Devices. (2016).

[129] M.J. Gallagher, A. Fridman, Plasma Reforming for H2-Rich Synthesis Gas, First Edit, Elsevier, 2011.

[130] L. Di, Z. Xu, K. Wang, X. Zhang, A facile method for preparing Pt/TiO2 photocatalyst with enhanced activity using dielectric barrier discharge, Catal. Today. 211 (2013) 109–113.

[131] J. Li, C. Ma, S. Zhu, F. Yu, B. Dai, D. Yang, A Review of Recent Advances of Dielectric Barrier Discharge Plasma in Catalysis, Nanomaterials. 9 (2019) 1428.

[132] X. Liu, Z. Liu, J. Zheng, X. Yan, D. Li, S. Chen, W. Chu, Characteristics of N-doped TiO2 nanotube arrays by N 2-plasma for visible light-driven photocatalysis, J. Alloys Compd. 509 (2011) 9970–9976.

[133] L. Ma, S. Hu, P. Li, Q. Wang, H. Ma, W. Li, In situ synthesis of sulfur doped carbon nitride with enhanced photocatalytic performance using DBD plasma treatment under H2S atmosphere, J. Phys. Chem. Solids. 118 (2018) 166–171.

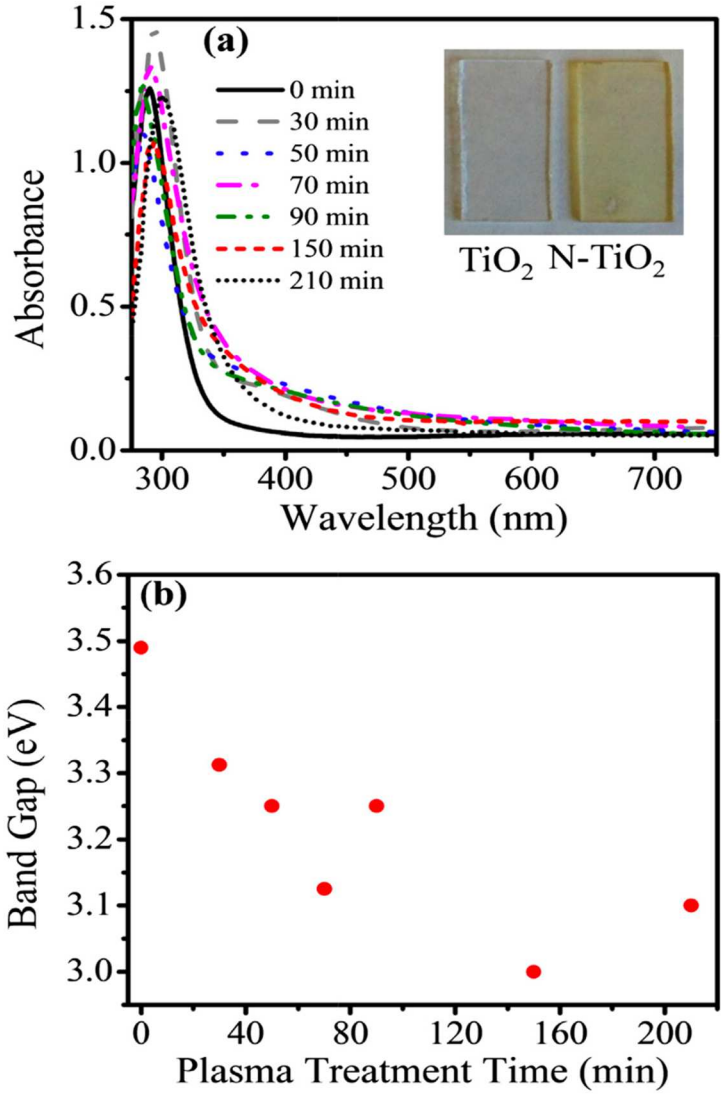

Fig. 1: (a) UV-vis spectra of undoped TiO_2 and plasma-treated nitrogen-doped TiO_2 (N-TiO_2) films with a variation of plasma treatment time and (b) variation of band gap with the time of plasma treatment [58].

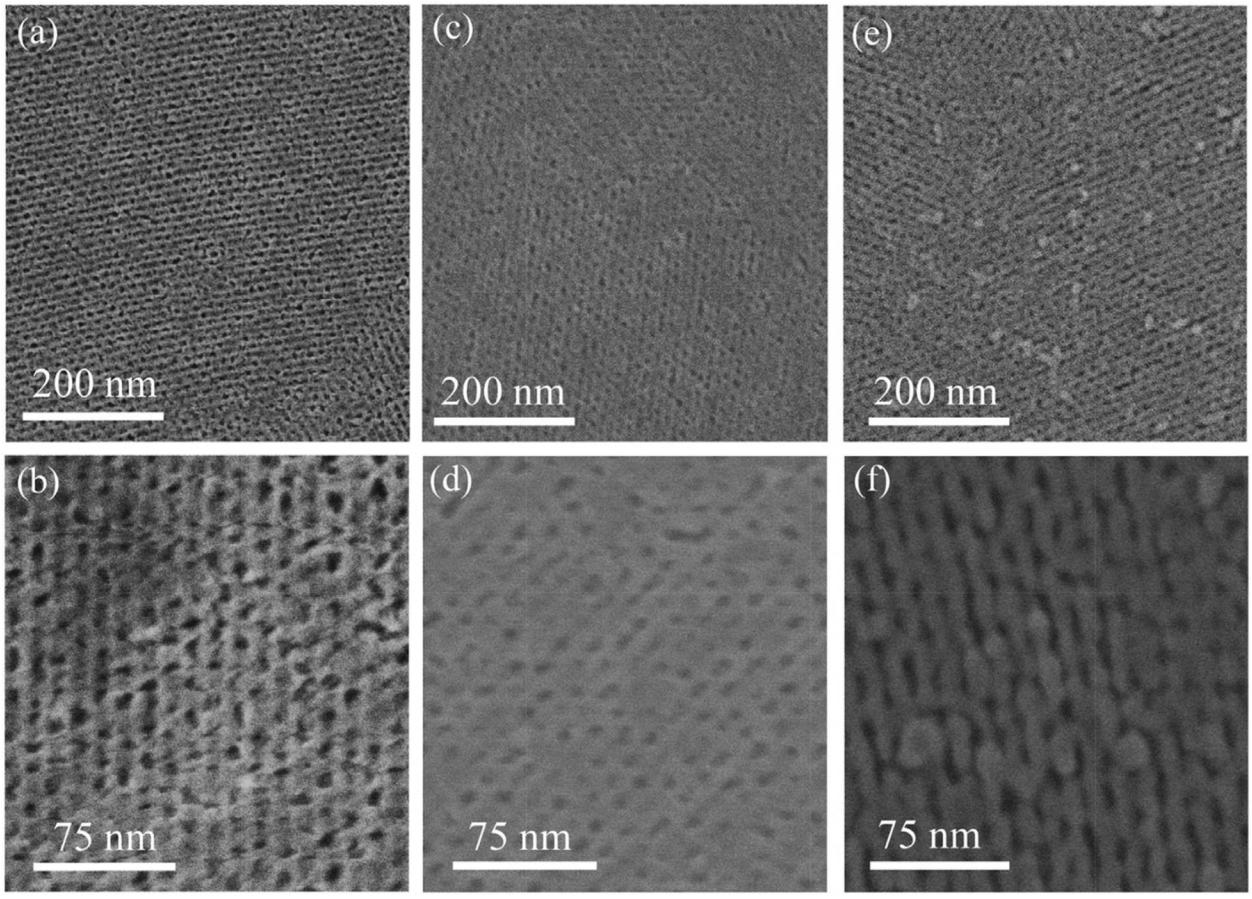

Fig. 2: SEM images of (a, b) undoped TiO_2 (c, d) 30 min plasma treated nitrogen-doped TiO_2 and (e, f) 210 min plasma treated nitrogen-doped TiO_2 films [58].

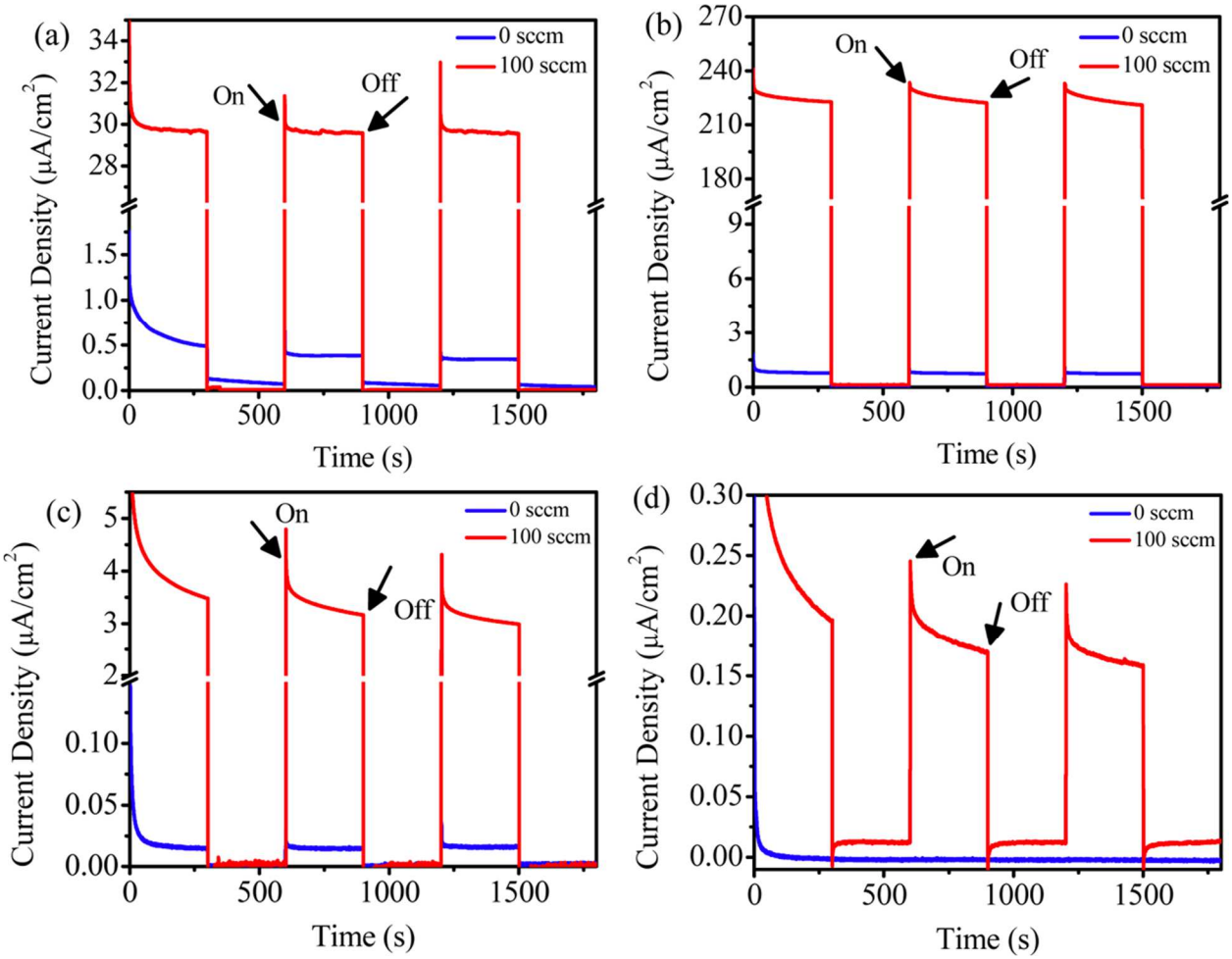

Fig. 3: Current density (micro A/cm^2) vs. time (s) profiles with 0 standard cubic centimeters per minute (sccm) nitrogen-doped TiO_2 (untreated) and 100 standard cubic centimeters per minute nitrogen-doped TiO_2 films under the illumination of (a) Xe arc lamp with AM 1.5 G filter, (b) UV-LED (UVLED), (c) blue-LED (BLED), and (d) green-LED (GLED) [44].

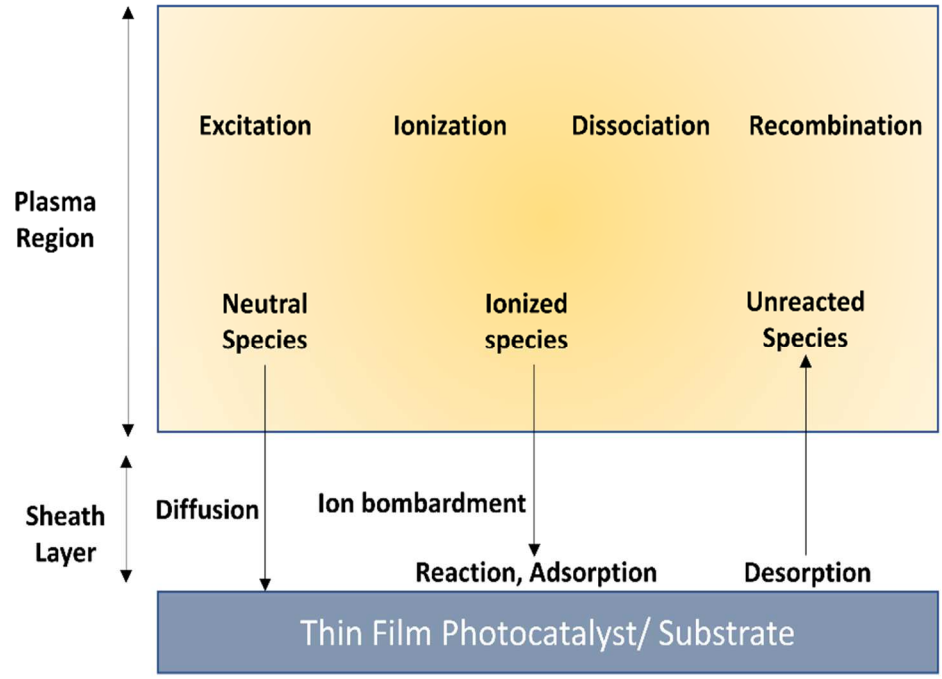

Fig. 4: The steps included in the plasma doping process in the PECVD reactors [66,115].

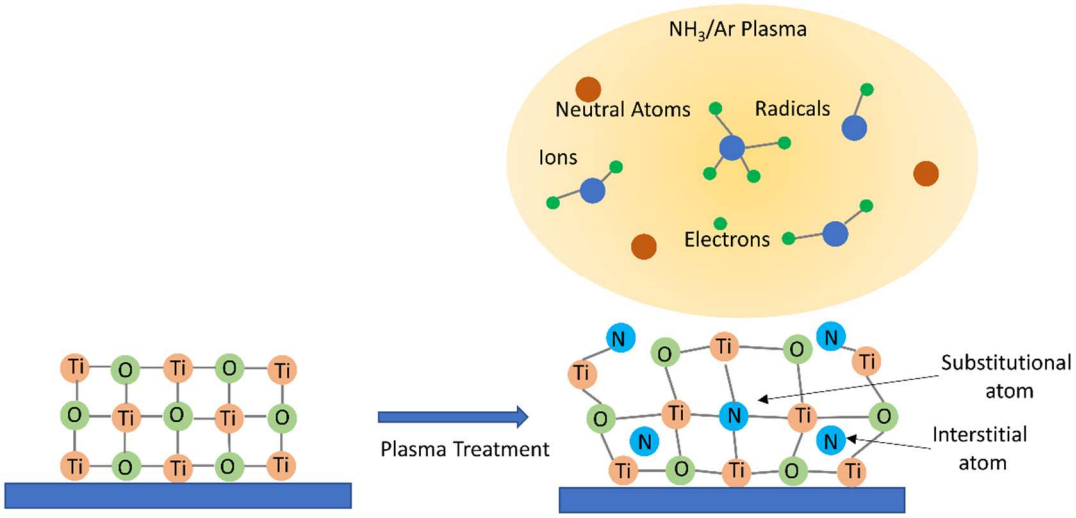

Fig. 5: Mechanism of Nitrogen doping of TiO_2 using NH_3/Ar plasma [67].

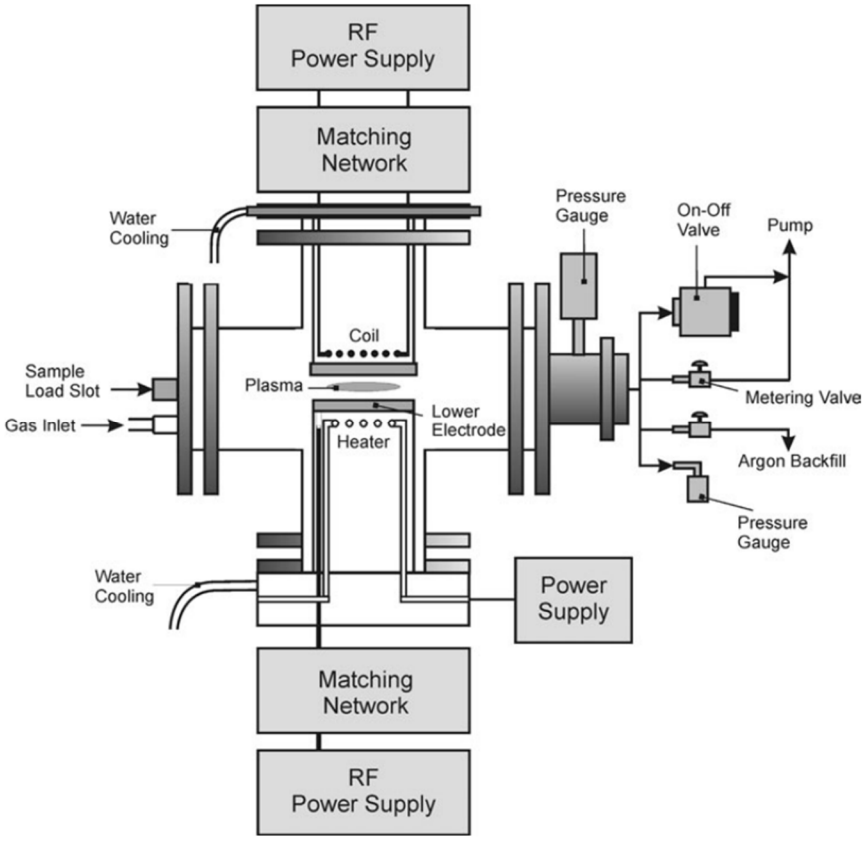

Fig. 6: Schematic of RFCVD plasma reactor with ICP [70].

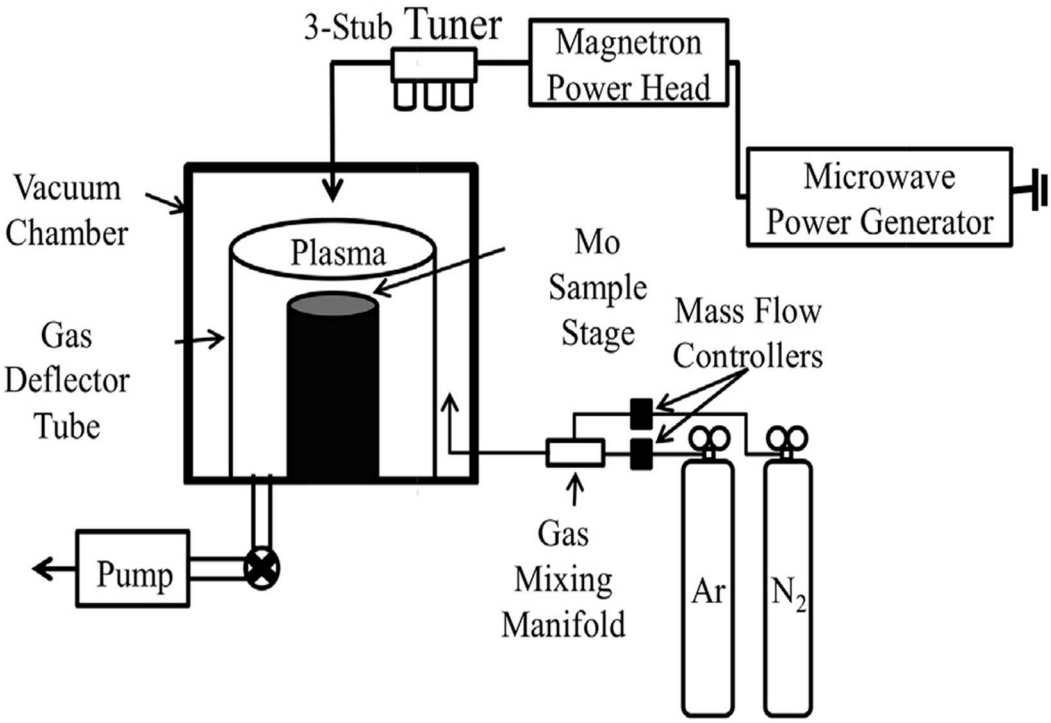

Fig. 7: Schematic of MPCVD reactor [58,111].

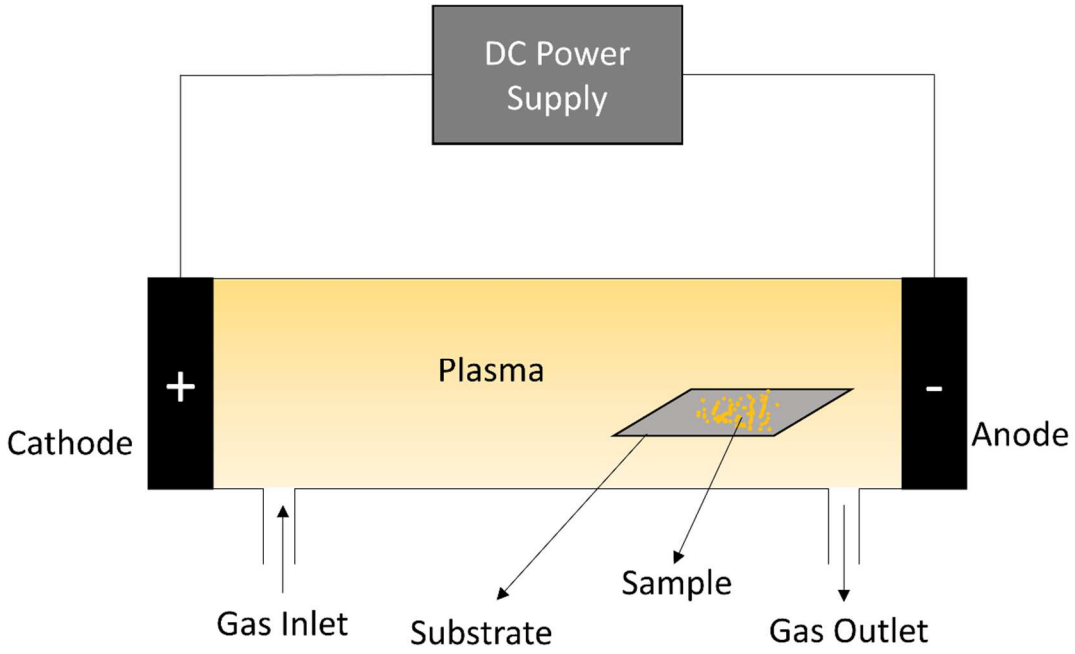

Fig. 8: Schematic of DC plasma reactor [87].

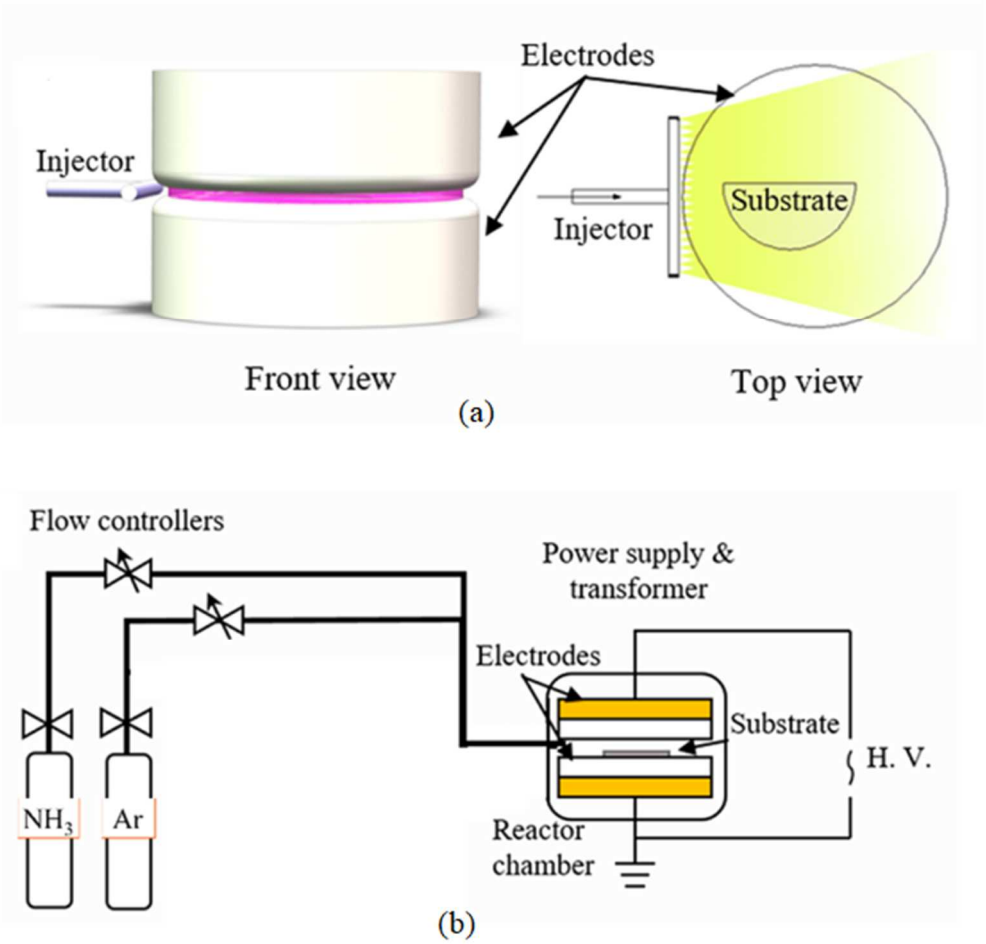

Fig. 9: Schematic of (a) DBD plasma discharge for doping, (b) experimental setup for DBD plasma doping [67].

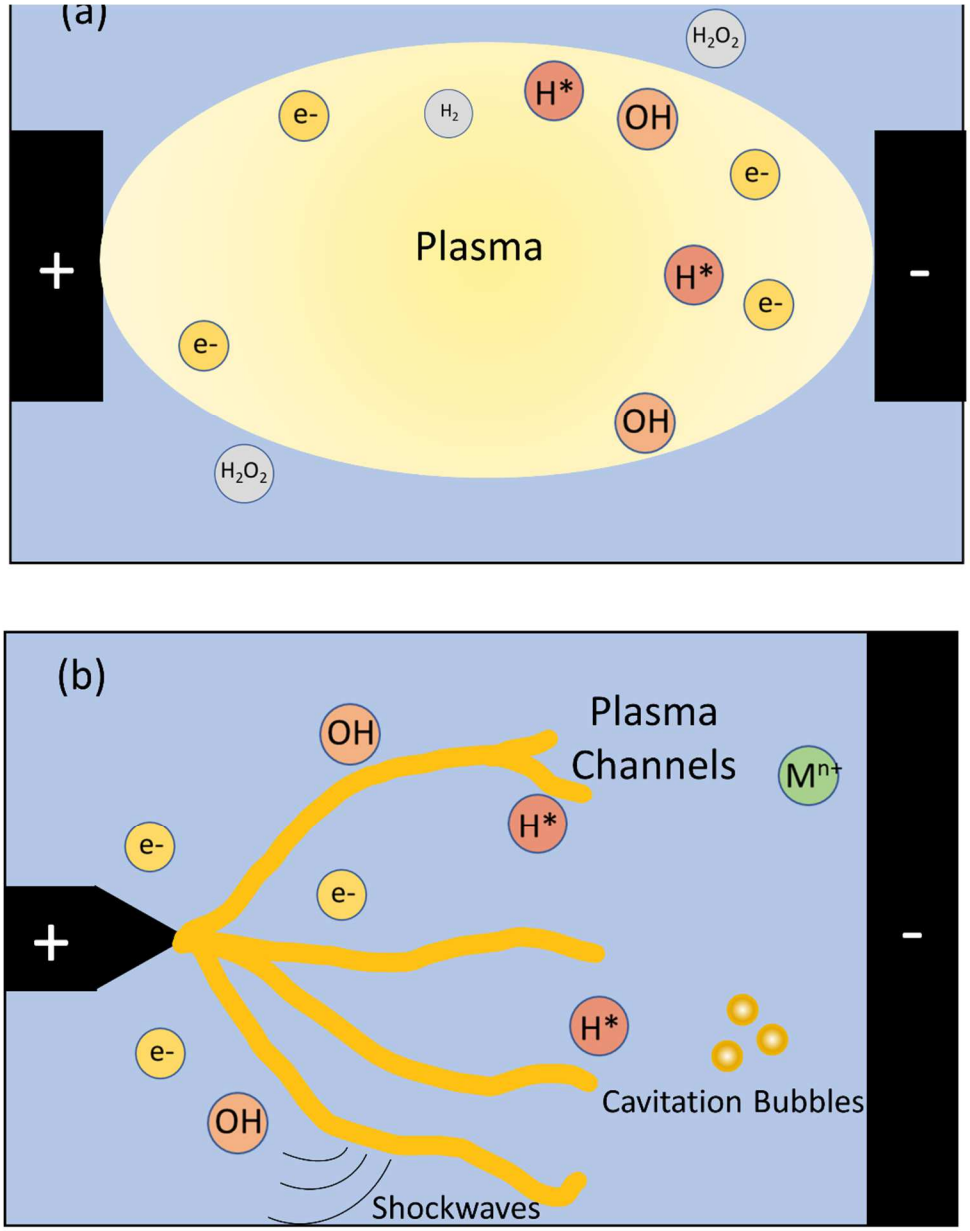

Fig. 10: LPP process for plasma generation for (a) plasma in a bubble, and (b) streamer plasma discharge [99].

1283

1284 **Table 1:** Descriptive analysis of several doping techniques.

Method	Description	Advantages	Disadvantages	Reference
Sol-gel	A wet chemical process involving hydrolysis and condensation reaction of precursors such as metal alkoxides and chlorides, with water or alcohol.	- practical, adaptable, easily controllable, no vacuum - can be assisted by other methods - low cost and simple operating requirements - homogenous and reproducible - yields high purity and desired stoichiometry	- time consuming - fracture on thin films - a long period of deposition - requires high chemicals - may pose challenges while incorporating a dopant precursor into a certain type of photocatalyst without damaging its structure	[116–119]

Method	Description	Advantages	Disadvantages	Reference
CVD	A thin film of metal oxide is formed by the materials and precursor condensation from a vapor phase to form a solid state.	- Excellent adhesively - generate uniformly distributed films - high density obtained along with controlled crystal structure and uniform films - increased corrosion and wear resistance	- high operating and capital cost - high reaction temperature - slow process - vacuum needed -nanostructure easily damaged due to high temperature	[116,120,121]
PVD	It involves physical processes such as evaporation, the collision of ions or sublimation, and the transfer of atoms from a solid or molten state to a surface.	- suitable for any type of inorganic materials - thermal evaporation process is protected from defect nucleation and damage although sputtering is not - enhanced hardness and	- high vacuum and temperature - slow and costly - additional cost of cooling system - impurity layer deposition - multiple steps required - high energy due to resistive heating	[116]

Method	Description	Advantages	Disadvantages	Reference
		resistance to oxidation and wear - environmentally approachable	and electrons beam - the high surface area of some photocatalysts may not be maintained due to high temperature - may pose challenges while incorporating a dopant precursor into a certain type of photocatalyst without damaging its structure	
Spray pyrolysis	An ionic solution containing the doping materials in the form of soluble salts is sprayed using a nanoporous uniformly distributed nebulizer onto the heated substrate in the furnace.	- can be operated at atmospheric pressure, maintain stoichiometry and homogeneity - multilayer fabrication capability - different precursors can be used - cheap and can be easily performed	- high flowrate can cause the heterogeneous coating - heating required for thermal treatment - may pose challenges while incorporating a dopant precursor into a certain type of photocatalyst without damaging its structure	[122,123]

Method	Description	Advantages	Disadvantages	Reference
Hydrothermal	This is a wet chemical process under mild reaction conditions by controlling reaction parameters such as temperature, pressure, pH, time, and surfactant.	- low energy requirement - simple equipment - controllable morphology - high-phase purity - size selective growth with small particle size	- costly autoclave required - at higher temperatures, clustering can happen - may pose challenges while incorporating a dopant precursor into a certain type of photocatalyst without damaging its structure	[124,125]

Method	Description	Advantages	Disadvantages	Reference
Plasma treatment	Fragmenting dopant precursor molecules using active plasma that deposit onto the photocatalyst surface	- no need for organic solvents and green technology - avoids catalyst poisoning - chemical, thermal, and mechanical stabilities - single step and less costly - pore-free and uniform films - low chemical consumption - dry process - less water and energy consumption	- relatively equipment cost	[58,126,127]

1285

1286

1287 **Table 2:** Advantages and disadvantages of various types of plasma.

Plasma Types	Advantages	Disadvantages	Application	Reference
PECVD (Plasma-Enhanced Chemical Vapor Deposition)	-Simple reactor -Vapor molecules break very easily - Facilitates the growth of films at a low-temperature substrate temperature -Reasonable deposition rate on films -The uniform surface of films -Highly pure	-Difficult to control the stoichiometry -Probable surface damage by ion bombardment -The possibility of contamination of particle and chemical - Relatively expensive -The system becomes complex as a pumping system is required for maintaining low pressure	-Microelectronics development -Fabrication of integrated circuits, solar cells, transistors, photovoltaic and photonic applications -Development of organic polymers and organometallic compounds -Biological applications such as immobilization of biomolecules, surface treatments of implants, and biomaterials	[66,128]
MPD (Microwave Plasma Discharge)	-High energy density and high ionization rate -Efficient use of input energy -Operation pressure can vary from millitorr to atmospheric pressure	-Can be complex and expensive to incorporate high-frequency power	-Syngas production system	[129]
RFPD (Radio Frequency Plasma	-No direct contact between plasma and electrode is needed	-	-Syngas production system	[129]

Discharge)				
DBD (Dielectric Barrier Discharge)	-Green & Efficient -No release of hazardous chemicals -Comparatively easier construction -Simple and easy operation -Fast and facile method -Improves property and enhances catalytic performance -Enhance distribution of metal nanoparticles	-Nonuniform, filamentary structure -Limited current, low temperature of the gas -Low power density -Additional energy requirement to preheat the reactant	-Quick and easy preparation of supported metal catalysts for energy and environmental application. -Mesoporous photocatalyst with enhanced activity -Automobile exhaust gas catalysis -CO_2 reforming of CH_4 -CO and CO_2 methanation -CH_4 conversion -Methanol photooxidation	[130,131]
LPP (Liquid Phase Plasma)	-Automatic production of reducing agents -No external addition of toxic chemical reducing and stabilizing agent so comparatively pure -Environment friendly -One-step, fast, and wide-scale synthesis process of nanomaterial -The presence of a novel plasma liquid interface -Physical and chemical parameters can	-Detailed spatial and temporal evolutions of the processes are not well understood	-Fabrication of different nanomaterials of various characteristics	[98,99]

	be controlled easily -Nanomaterial nucleation and growth can be controlled -Composition, size, and shape of nanomaterial can be finely tuned -No gas, pumping system, or water-cooled vacuum chamber is needed, so less costly			
Arc Discharge	-Insensitive to changes in environment and pressure -Simple operation -Can provide the high temperature needed for gasification -High production rate -High-quality product -Comparatively less impure product	-High electric energy requirement, so costly -Expensive equipment	-Fuel conversion	[9,129]
Ion Implantation	-Doping dosage and depth can be controlled -Uniform surface -A wide range of operating temperature -Less impurity	-More expensive equipment -A high requirement for energy input -Non-uniform		[9]
Corona Discharge	- Efficient power transfer into the plasma discharge -Satisfactory spatial uniformity		-Catalytic effect in combustion and fuel conversion	[129]

1288

1289 **Table 3:** Photocatalysts doped with various dopants using plasma treatments for environmental applications.

Types of Plasma	Photocatalyst	Plasma treatment method	Scope	Effects of plasma	Reference
N_2 non-thermal plasma/cold plasma	N-TiO_2	N-TiO_2 treated in DBD reactor for 30min at 15W, N_2 flow rate 450mL/min	Methyl orange degradation	-Bandgap was reduced to 1.7 from 3.0 eV for bare TiO2 -higher substitutional N and surface O_2 -2.8 times higher reaction rate and -13-35% higher degradation rate compared to conventional N-TiO_2 (without plasma treatment)	[65]
	Nanoporous TiO_2	RF generator used with Ar as carrier gas and N_2 as reactive gas	-Organic dye degradation -Medical application as an antibacterial	- Increment of surface energy -Reduction of band gap energy to below	[107]

			agent	3.2 eV -High photostability and durability	
	TiO_2 nanotube arrays	A quartz tube of 2.2cm inner diameter acted as a reactor at 200 Pa pressure		-Better photocatalytic activity -A facile transformation from anatase to rutile phase at the low annealing temperature -Greater photocurrent density	[132]
N_2/Ar plasma	TiO_2	MPCVD system purged with Ar at 100 sccm and N_2 at 40 sccm	-Degradation of methylene blue dye under visible light -Water oxidation activity enhancement	- 18% reduction of specific surface area -Uniform N_2 distribution through the depth of the film -Dye degradation rate coefficient increased by 6 times	[58]

Ar/O_2 plasma	$Cu\text{-}TiO_2$	Atmospheric pressure thermal plasma with a DC non-transferred plasma torch	Preparation and doping of nano-catalyst for gaseous elemental Hg removal	-single step surface modification -clean nanoparticle surface -Cu species highly distributed in TiO_2 -enhanced conductivity and electron trapping	[109]
H_2 cold plasma	$Ag/N\text{-}TiO_2$ nanotube	The sample was placed in a DBD reactor where $Ar\text{-}H_2$ is pumped at 50 L/min for 5 min	Green and efficient synthesis of photocatalyst	-Ag nanoparticles evenly distributed on the inner walls of nanotubes -small particle size of 5.8nm	[64]

Eu (Liquid Phase Plasma)	TiO_2	Powder TiO_2 and Eu precursor dispersed in a cylindrical quart batch reactor and direct pulse type plasma used to prevent corrosion of electrodes	-Mineralization of acetylsalicylic acid -Decomposition of environmental pollutants	-Eu uniformly precipitated on the TiO_2 surface from the precursor -A shift of the Raman peak to a higher wavelength -Higher photocatalytic efficiency -Atomic oxygen % increased -Bandgap energy reduction from 3.18 to 3.03 eV	[103]
Tungsten oxide (Liquid Phase Plasma)	TiO_2	Tungsten hexachloride was added to the solution of ethanol and deionized water and 0.5g TiO_2 was added later	Degradation of diethyl phthalate	-Specific surface area reduction by blocking mesopores -Enlarged pore diameter -Improvement of photocatalytic	[109]

				activity -Reduction of intrinsic bandgap energy -1.7 to 6.2 times more degradation under blue light	
Mo/V/W	Commercially pure TiO_2	In an immobilized photocatalytic surface doping materials were added to TiO_2, PEO (Plasma electrolytic oxidation) treated for 8 min with 150 mA/cm^2 current density	Can be repeatedly used for textile wastewater treatment	-Suppressed the formation of rutile -Higher number of pores on the surface and active surface area -High charge separation efficiency, low recombination rate -Increased mineralization of MB dye	[108]

N_2 plasma	CdS/N-CoSx	CoSx polyhedrons were placed in a plasma chamber (RF 13.56 MHz. 45W) and N_2 flow at 100 Pa, followed by the solvothermal method	Cr(VI) reduction	-Enhanced surface wettability and conductivity -Facilitates Co-N bond -5 min plasma treatment shows the best photocatalytic activity	[110]
H_2S plasma	S-doped g-C_3N_4	DBD reactor was operated at a constant flow of H_2S (40 mL/min) and a voltage of 10 kV	Degradation of Rhodamine Blue (RhB) dye	-Larger surface area and narrower band gap - Maximum degradation of 98% was obtained	[133]

1294 **Table 4:** Photocatalysts doped with various dopants using plasma treatments for energy and other applications.

Types of Plasma	Photocatalyst	Plasma treatment method	Scope	Effects of plasma	Ref.
N_2 Plasma	N- TiO_2	DBD plasma reactor used quartz, pressure 1 bar, power frequency 6 kHz, 300 ml/min gas flowrate	Photocatalysis	-More oxygen vacancy and Ti^{3+} ions found - Rate of hydrogen evolution found to be 8.1 $mmol.h^{-}.g^{-1}$ -Narrower bandgap	[112]
CH_4 Plasma	C-doped Co_3O_4	RF (13.65 MHz) plasma	HER and OER	-Oxygen vacancies and heteroatom - The plasma treatment enhanced HER - For the same current density, 65% and 26% reduction of overpotential was found for HER and OER respectively	[71]

N_2 Plasma	N doped Magnetic WO_{3-x}-@Mesoporous carbon	High DC voltage (1200 V)	H_2 production and antibiotic degradation	-Larger surface area and band gap reduced to 2.08 eV - The H_2 production increased to 2765 $\mu molg^{-1}h^{-1}$ - About 90% degradation of antibiotics	[87]
H_2	Mesoporous black TiO_2 thin film	TiO_2 film purged with H_2 at 100 sccm and in MPCVD system for 10 min at 5 torr pressure	Photoelectrochemical water oxidation	-Scattering length density (SLD) reduction, so, significant H_2 uptake -Improved interfacial charge transfer and restricted recombination -larger specific surface area	[111]
N_2/Ar Plasma	Mesoporous N-TiO_2 thin film	The sample was placed on the evacuated Mo sample stage, purged with Ar at 100 sccm, and in the MPCVD system, varying N2 flowrates	Photoelectrochemical water oxidation	-Enhancement of photocurrents (up to 80-240 times) -Significant enhancement of water oxidation (up to a maximum of 7 times) -Bandgap reduction from 3.5 to 2.88 eV	[44]

N_2 plasma	N-Cu_2O/CuO	Nano-catalyst powder inside a plasma chamber with N_2 flow rate at 50 sccm and 100 Pa	H_2O_2 generation	-No need for precious metal or organic scavengers -Improved charge separation ability -CuO on the surface acts as an active site for more photo-generated electrons -3 and 8 times more H_2O_2 production was obtained with plasma treated N-Cu_2O/CuO compared to Cu_2O and CuO, respectively.	[45]
N_2 plasma	Fe: ZnO nanowires	Chemical vapor deposition chamber used with plasma power 500 W for 10 min	Photoelectrochemical, photovoltaic, photo-response of ZnO wires	-Increased photoconductivity of the film -bandgap reduction from 3.261 to 3.25 eV -The presence of a high density of shallow donor states -Reshape the conduction band -Passivation of oxygen vacancy -Dissociation of weakly bonded nanowires -Reduction of the density of nanowire surface area	[113]

1295